

DOI: 10.1002/adem.201500333

# Thermoelectric Devices for Power Generation: Recent Progress and Future Challenges\*\*

By Qi Hao Zhang, Xiang Yang Huang, Sheng Qiang Bai, Xun Shi,  
Ctirad Uher and Li Dong Chen\*

*Thermoelectric (TE) devices for power generation have been attracting increasing attention on account of their advantages such as solid-state operation, good stability, and high reliability. This paper presents an overview of the design principle, fabrication methods and testing technology of TE power generation devices. Particular attention is paid to skutterudite-based devices regarding electrode fabrication, barrier layer design, interface optimization, protective coating, and evaluation of elements and modules. The development of Bi<sub>2</sub>Te<sub>3</sub>-based devices for power generation focusing specifically on the optimization of Bi<sub>2</sub>Te<sub>3</sub>/electrode joints and fabrication and evaluation of Bi<sub>2</sub>Te<sub>3</sub>-based modules is summarized. The future challenges concerning TE devices for power generation are discussed.*

## 1. Introduction

Traditional non-renewable energy sources have become increasingly exhausted with the ongoing unsatiable thirst for energy to satisfy human consumption and industrial activities. The search for and exploitation of new, cleaner, more

sustainable energy sources, and improvements in the existing energy efficiency, therefore, are highly desirable. Among all viable technologies addressing this issue, thermoelectric (TE) energy converters, which can convert thermal energy into electrical energy, have attracted considerable attention because of their advantages of solid-state operation, no mechanical moving parts, no release of greenhouse gases, good stability, high reliability, and long operating life.<sup>[1]</sup> The solid-state TE devices can both transform heat into electric power using the Seebeck effect and, conversely, change electrical energy into thermal energy to enable cooling or heating using the Peltier effect. They have been utilized or are at the trial stage in fields such as military, aerospace, transportation, medical services, electronics, temperature detecting and measuring instruments and, generally, meeting the demands for energy conservation and environmental protection.<sup>[2]</sup>

TE materials as the core component of TE devices play a decisive role in the operation of TE devices. The efficiency of TE materials is determined by a dimensionless figure of merit, defined as  $ZT = (\alpha^2 / \rho\kappa)T$ , where  $\alpha$  is the Seebeck coefficient,  $\rho$  is the electric resistivity,  $\kappa$  is the thermal conductivity and  $T$  is the absolute temperature. An ideal TE material should combine a large  $\alpha$  to create a large potential difference, a low  $\rho$  to minimize the Joule heating and a low  $\kappa$  to maintain a large temperature gradient between the hot and cold sides of the couple. The energy conversion efficiency of a TE device is proportional to the Carnot efficiency and the  $ZT$  values of TE

[\*] Prof. L. D. Chen, Q. H. Zhang, Dr. X. Y. Huang, Dr. S. Q. Bai, Prof. X. Shi

State Key Laboratory of High Performance Ceramics and Superfine Microstructure, Shanghai Institute of Ceramics, Chinese Academy of Sciences, Shanghai 200050, China

Q. H. Zhang  
University of Chinese Academy of Sciences, Beijing 100049, China  
Prof. C. Uher

Department of Physics, University of Michigan, Ann Arbor, Michigan 48109, USA

Prof. L. D. Chen  
Shanghai Institute of Materials Genome, Shanghai 200444, China  
E-mail: cld@mail.sic.ac.cn

[\*\*] The authors gratefully acknowledge the supports from National Basic Research Program of China (973 Program) under Project No. 2013CB632504, the research grant (No. 15JC1400301) from Shanghai government and International S&T Cooperation Program of China (Grant No. 2015DFA51050).



*Dr. Xiang Yang Huang is an associate professor at the Energy Materials Research Center, Shanghai Institute of Ceramics, Chinese Academy of Sciences, China. He received his PhD degree in materials science from Tongji University in 2004. He worked at Tohoku University as a Core Researcher for Evolutional Science and Technology researcher from 2004 to 2008. His research interests focus on the design and fabrication of thermoelectric module and novel synthetic techniques for high performance thermoelectric materials.*



*Dr. Sheng Qiang Bai is a senior engineer and deputy head of the Thermoelectric Research Team in Shanghai Institute of Ceramics, Chinese Academy of Sciences (SICCAS). He received his bachelor degree from Zhejiang University in 2001, and his PhD from SICCAS in 2010. In 2001, he joined SICCAS and was promoted to senior engineer in*

*2010. His research activities primarily involve the mass production of  $\text{CoSb}_3$ -based skutterudites; design and fabrication of thermoelectric devices from  $\text{Bi}_2\text{Te}_3$ -based alloys,  $\text{CoSb}_3$ -based skutterudites, half-Heusler alloys, and  $\text{SiGe}$ -based alloys; evaluation the service behavior of thermoelectric devices; design and fabrication of thermoelectric generators; thermoelectric cooling and heating systems.*



*Dr. Li Dong Chen received his PhD degree in Materials Science from Tohoku University in 1990 and joined Shanghai Institute of Ceramics, Chinese Academy of Sciences as a professor in 2001. He has published over 300 authored or co-authored papers in the area of inorganic materials and composites. His research activity mainly focuses on the design,*

*synthesis, and characterization of thermoelectric materials, as well as the integration of thermoelectric devices. For his contributions, he has received numerous awards including the research progress award of Japan Powder and Powder Metallurgy Society, GM Foundation Science & Technology Achievement Award (First Prize), State Science and Technology Awards of China.*

materials. For example, a TE power conversion device with material's  $ZT$  of 3 would yield about 50% of the Carnot efficiency when operating under  $500^\circ\text{C}$  for the hot side and maintaining the cold side at  $30^\circ\text{C}$ .<sup>[3]</sup> Figure 1 shows the time line the maximum  $ZT$  has achieved and highlights the recent progress made with novel more efficient TE materials. Since the middle of the 20th century, narrow band semiconductors have been widely studied as TE materials of choice because of their high Seebeck coefficients and the heat conduction dominated by phonon transport.<sup>[4]</sup>  $\text{Bi}_2\text{Te}_3$  was first discovered by Goldsmid in 1954 and semiconductor alloys such as  $\text{Bi}_x\text{Sb}_{2-x}\text{Te}_3$ ,  $\text{PbTe-PbSe}$ , and  $\text{Si}_{0.8}\text{Ge}_{0.2}$  were subsequently developed into useful TE materials following extensive studies by Ioffe et al. who demonstrated that short-range order disturbances (alloy scattering) could very effectively scatter heat-conducting phonons and cause dramatic reductions in the lattice thermal conductivity without causing much damage to the carrier mobility.<sup>[5-7]</sup> From the 1960s to 1990s, however, attempts to improve  $ZT$  did not materialize and the maximum  $ZT$  values stagnated near unity in the  $(\text{Bi}_{1-x}\text{Sb}_x)_2(\text{Se}_{1-y}\text{Te}_y)_3$  alloy family.<sup>[8]</sup> Fortunately, research efforts to improve TE materials picked up after the 1990s due to new conceptual developments, renewed interests in the theory of transport phenomena, and the desire to address energy crisis with the aid of solid-state energy conversion technology.<sup>[1,2,9-17]</sup> Over the past two decades, the maximum value of  $ZT$  has constantly reached new highs for different families of TE materials. For example,  $ZT$  of 1.4 was achieved in p-type nanocrystalline  $\text{BiSbTe}$  bulk alloys,<sup>[18]</sup> 1.7 with multiple-filled skutterudites,<sup>[19]</sup> 1.5 for "phonon-liquid electron-crystal" structured  $\text{Cu}_{2-x}\text{Se}$ ,<sup>[20]</sup> 1.7 for  $\text{Cu}_{2-x}\text{S}$ ,<sup>[21]</sup> 1.5 for half-Heusler alloys,<sup>[22-24]</sup> 2.2 for bulk TE materials with all-scale hierarchical architectures,<sup>[25]</sup> and 2.6 for SnSe single crystals<sup>[26]</sup>. TE materials have thus been developed into a big family, including materials encompassing semimetals, semiconductors, ceramics, oxides, and polymers, possessing various crystalline forms from monocrystals and polycrystals to nanocomposites and

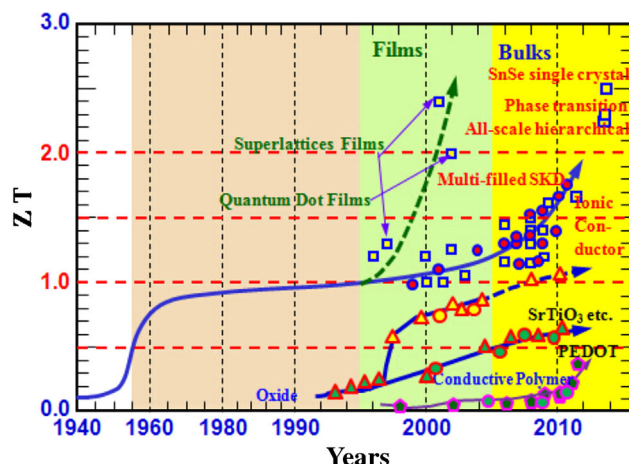


Fig. 1. Histogram of the maximum  $ZT$  values documenting the recent progress made with novel thermoelectric materials.

covering different dimensionalities from bulk to films to wires and to clusters.<sup>[27]</sup>

The continuous development of new materials and the upsurge in  $ZT$  values provide the material support for the development of TE devices. However, industrial applications place increasingly higher demands on TE devices, especially regarding large-scale applications intended for power generation. To construct an optimal TE device, there are three key factors to be satisfied: efficiency, service operation and cost. In order to achieve higher efficiency, several issues should be taken into consideration beyond having TE materials with high  $ZT$  values. First, high  $ZT$  values are needed over a broad range of temperatures in order to achieve the maximum energy conversion efficiency. TE materials typically have quite a restricted temperature range where the figure of merit is maximized and the performance declines sharply outside of this range. In order to overcome this limitation, many approaches have been tried, such as designing crystals with a gradient of charge carrier concentration, constructing segmented TE modules, and adopting multi-stage structures.<sup>[28,29]</sup> The second issue concerns the interfacial thermal/electrical resistance which should be minimized as much as possible, so that the degradation of the conversion efficiency can be alleviated and high reliability of TE devices is maintained. Finally, the proper structure design, including that of heat exchangers, is crucial to the performance of TE devices as the efficiency is sensitive to the device dimensions for a given interfacial thermal/electrical resistance values.

Improving the conversion efficiency is the top priority for TE power generation devices. Beyond that, the service behavior (stability and reliability) has to satisfy the requirements of practical applications. High reliability is considered as the chief advantage of TE devices. However, due to the influence of external factors such as the methods of synthesis, assembly of modules, and the working environment, TE devices may still face a failure. One reason for the failure is migration of chemical species, which happens frequently at the joints of TE modules. Elements which diffuse into the TE materials often act as additional dopants, resulting in the performance degradation.<sup>[30]</sup> Another reason is that the strength of TE devices decreases under fatigue loading, exerting negative influence on the service life of TE devices.<sup>[31]</sup> Therefore, to improve the stability and reliability of TE devices becomes another important issue to be addressed.

Besides the energy conversion efficiency and service behavior, the cost of generating electricity is of comparatively equal importance when considering commercial applications of TE devices.<sup>[32,33]</sup> The cost of TE devices stems from three aspects: the cost of raw materials, material processing cost, and module processing cost. Compared with photovoltaic or other solid-state conversion, TE devices still cost more. Therefore, only after achieving cost reductions, TE power generation can become an alternative to these power sources for a wide range of applications.<sup>[34]</sup>

Although, sustained efforts in research and development of TE materials in both academia and industry have been made

over the past years, the pace of module development still lags relatively behind and fails to meet the needs of industrial TE applications such as waste heat recovery and its conversion to electricity<sup>[35–39]</sup> and many other prospective areas. This deficiency mainly concerns aspects such as device efficiency, power density, service performance, cost, and large-scale production. In this review, the design principle, fabrication methods, and testing technology of TE power generation devices will be presented. The focus will be primarily on power generation using skutterudite (SKD)-based materials and modules based on bismuth telluride (BT). The advances in filled-SKD-based TE devices including aspects such as electrode fabrication, barrier layer design, interface optimization, protective coating, and evaluation of the elements and modules will be summarized. The development of BT-based devices for power generation will be assessed with respect to the optimization, fabrication and evaluation. In view of the complexity of the cost, this aspect will not be covered in this work. Future development trends and challenges for the TE power generation devices will be presented last.

## 2. Design Principle, Fabrication Methods, and Testing Technology of TE Devices

### 2.1. Configuration of TE Modules

The TE module is a solid-state energy converter that consists of a bunch of TE uni-couples wired electrically in series (or partly parallel) and thermally in parallel. Basic requirements for selecting a specific module configuration are to capture the heat most efficiently and provide for maximum module reliability. The structure of a conventional TE module follows the  $\Pi$ -shaped configuration shown in Figure 2a.<sup>[1,2]</sup> It consists of the column-like or cube-like n- and p-type TE elements connected electrically in series and thermally in parallel. The TE elements are sandwiched between two polymer or ceramic plates which serve as electrical insulators and thermal conductors. The  $\Pi$ -shaped module is applicable to situations where the heat flow is perpendicular to the plates.

In applications such as capturing heat from the exhaust gas, the heat flows along a cylinder and, hence, to attach a TE power generator made from the  $\Pi$ -shaped modules around a cylindrical heat source becomes extremely complicated.<sup>[40]</sup> This is especially so when the diameter of the cylindrical heat source is less than 1 cm. In that case, a tube-shaped module becomes a better option. As shown in Figure 2b, the tube-shaped module is assembled with a number of n- and p-type ring-shaped TE elements in a coaxial arrangement.<sup>[41]</sup> These ring-shaped TE elements are connected electrically in series and joined alternately at their inner and outer perimeters by interleaved ring-shaped electrodes. The gaps between n- and p-type ring-shaped TE elements both underneath and above the ring-shaped electrodes are filled with electrically and thermally insulating materials. The tube-shaped module has its inner tube surface as one thermocouple junction and the

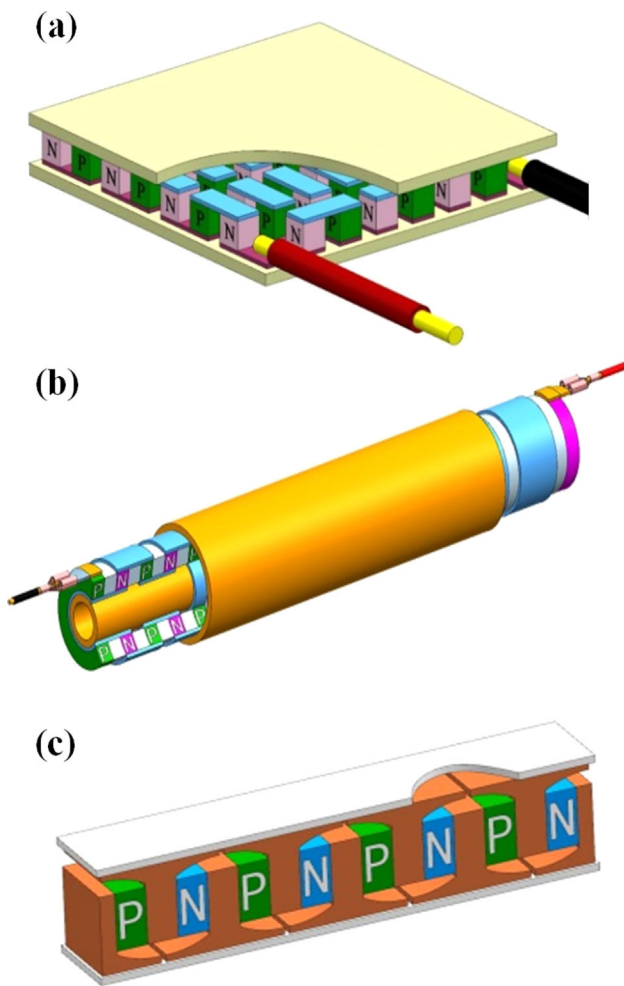


Fig. 2. Schematic diagram of (a)  $\Pi$ -shaped module, (b) tube-shaped module, (c) Y-shaped module.

outer as the other. In principle, both the inner surface and the outer surface ought to possess an electrically insulating and thermally conducting liner whose functions are the same as those of the ceramic plates used in the  $\Pi$ -shaped module. When the heat flows through the TE tube, either the outer surface or the inner space depending on the design, a temperature difference can be established and, consequently, the electrical power is generated

Not only specific application needs but also the properties of TE materials such as the coefficient of thermal expansion (CTE) play an important role in the design of TE modules. Figure 2c shows another novel Y-shaped configuration that can more readily accommodate TE elements with different thickness, area, and CTE.<sup>[42]</sup> Each column-like or cube-like TE element is sandwiched between the connectors. The connectors not only provide an electrical path from one TE element to another but also facilitate a thermal path from the fluid-carrying channels to the TE elements. In the Y-shaped configuration, the electrical current runs parallel to both the heat and sink sources, allowing for integration of TE materials with multiple geometries. Each TE element can be optimized

semi-independently, which is particularly favorable for a segmented module. Specifically, each p- and n-type leg can have a different cross-sectional area and/or thickness with each layer optimized to have the highest ZT in each particular temperature range. This combats negative influences of any compatibility mismatch on the optimum power output when the maximum efficiency of different element segments occurs at significantly different current densities.<sup>[43]</sup> In addition, the Y-shaped connector provides a shorter electrical path between the adjacent TE elements and a larger area between the heat (or sink) source and the connector.

## 2.2. Efficiency and Output Power of TE modules

Choosing an appropriate configuration based on the heat source and TE materials is the starting point in the design of modules used in particular situations. Subsequently, the interface design and geometry optimization are generally the most important issues. For the design of  $\Pi$ -shaped modules, the power output and the conversion efficiency are used to evaluate the module performance when operating in the power generation mode.<sup>[44]</sup> Here, we take a  $\Pi$ -shaped TE uni-couple as an example. Assuming that the dimensions (the length and the cross-section) of the two legs are equal and the TE performance is independent of temperature, the maximum conversion efficiency can be expressed as

$$\eta_{\max} = \frac{T_H - T_C}{T_H} \cdot \frac{\sqrt{1 + [Z]T_{ave}} - 1}{\sqrt{1 + [Z]T_{ave}} + \frac{T_C}{T_H}} \quad (1)$$

where  $[Z] = \frac{[\alpha]^2}{[\kappa][\rho]}$  ( $[\alpha]^2 = (\alpha_p - \alpha_n)^2$ ,  $[\kappa] = \kappa_p + \kappa_n$  and  $[\rho] = \rho_p + \rho_n$ . The subscript p and n denote the p- and n-type TE materials, respectively).  $T_H$  is the hot side temperature,  $T_c$  is the cold side temperature, and  $T_{ave}$  is the average temperature of the hot and cold sides, respectively. The maximum power output of such a  $\Pi$ -shaped TE uni-couple is defined as the power output generated when the uni-couple resistance matches the load resistance, which is expressed as

$$P_0 = \frac{[\alpha]^2 \Delta T^2 A}{4[\rho]L} \quad (2)$$

where  $\Delta T$  is the temperature difference between the hot and cold sides and  $A$  and  $L$  are the cross-sectional area and the length of the TE legs, respectively.<sup>[2]</sup> However, a realistic evaluation of the device performance should include the contact properties, as interfacial thermal resistance (ITR) and interfacial electrical resistance (IER) could exert a significant influence on the TE conversion efficiency and the power output. When the contact effects are taken into account, the maximum power output can be rewritten as

$$P_c = \frac{[\alpha]^2 \Delta T^2 A}{4[\rho](n + L)(1 + 2rl_c/L)^2} \quad (3)$$

Here,  $r = [\kappa]/2\kappa_c$  and  $n = 4\rho_c/[\rho]$  are referred to as the thermal and electrical contact parameters, where  $\kappa_c$  is the effective thermal conductivity of the contact layer,  $\rho_c$  is the contact electrical resistivity,<sup>[2,45]</sup> and  $l_c$  is the thickness of the contact layer. The effect of the contact can be easily found from the parameter  $P_i = P_c/P_0$ . As a result,

$$P_i = \frac{1}{(1 + \frac{n}{L})(1 + 2r \frac{l_c}{L})^2} \quad (4)$$

The corresponding conversion efficiency under the maximum power output is then expressed as

$$\eta = \frac{\left(\frac{T_H - T_C}{T_H}\right)}{\left(1 + 2r \frac{l_c}{L}\right)^2 \left(2 - \frac{1}{2} \left[\frac{T_H - T_C}{T_H}\right] + \left[\frac{4}{[Z]T_H}\right] \left[\frac{L+n}{L+2rl_c}\right]\right)} \quad (5)$$

Figure 3a illustrates the effect of the electrical contact parameter  $n$  on the power output ratio  $P_i$ . Apparently, the electrical contact resistivity has an important impact on the power output, especially for TE elements with short lengths. The corresponding conversion efficiency under the maximum power output of a realistic power generation TE device with different thermal contact resistance as a function of the length of TE elements for  $T_H = 527^\circ\text{C}$  with  $T_C$  at  $27^\circ\text{C}$  is shown in Figure 3b. It is obvious that the conversion efficiency  $\eta$  increases as the length of TE elements gets larger, while the interfacial thermal resistance significantly reduces conversion efficiency especially when the TE element length is relatively short. Clearly, the conversion efficiency is sensitive to device dimensions for given IER and ITR values. Therefore, appropriately selecting the contact materials and forming good electrical and thermal contacts are important factors in the design and fabrication of TE devices.

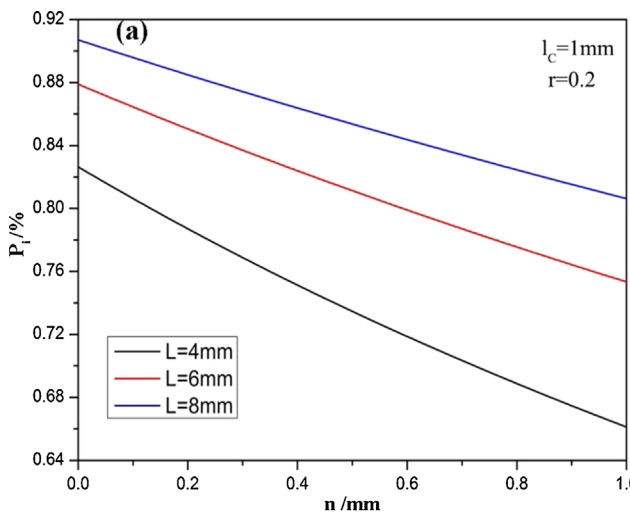


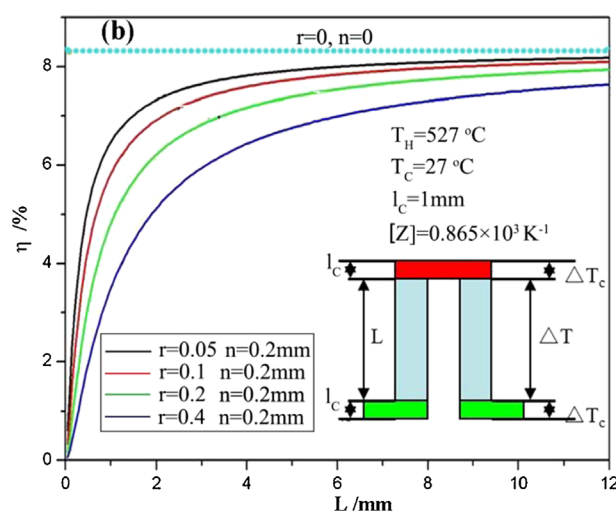
Fig. 3. (a) Power output ratio  $P_i$  as a function of the electrical contact parameter  $n$ , (b) the corresponding conversion efficiency under the maximum power output as a function of TE element length for different thermal contact parameter  $r$ .

### 2.3. Fabrication of TE Elements and Modules

Figure 4 shows the schematic diagram of a typical  $\Pi$ -shaped TE uni-couple, which is composed of one n-type semiconductor, one p-type semiconductor, intermediate layers and electrodes. The uni-couple is covered with a protective coating to minimize the degradation of TE materials at elevated operation temperatures. Each leg named as "TE element" has electrodes at both the hot side and the cold side. In order to relax the stress at the joint and prevent inter-diffusion between the electrode and the TE semiconductor, an interlayer or a barrier layer is usually employed. In the past several decades, a number of attempts have been made to join TE materials onto different electrodes with different barrier layers.

#### 2.3.1. Soldering

The soldering technique is a cost-effective, mature and industry-scalable manufacturing process that has been widely used in preparing various TE refrigeration modules. In commercial BT modules, soldering is usually employed to bond the columns to the electrode (usually copper). However, TE modules assembled with low temperature solders have limited service temperatures beyond which the solder becomes molten and severe diffusion of the solder into the BT material takes place.<sup>[46]</sup> Different kinds of solder alloys, as listed in Table 1, have been developed and used to improve the contact performance. For the preparation of high-temperature TE elements and modules, the solder with the higher melting point is needed. For example, fluxless  $\text{Zn}_{78}\text{Al}_{22}$  solder bars (melting point  $482^\circ\text{C}$ , Harris Products) and its flux paste were used for a SKD-based module which was assembled with nine pairs of n-type  $\text{Yb}_x\text{Co}_4\text{Sb}_{12}$  and p-type  $\text{Ce}_x\text{Fe}_3\text{CoSb}_{12}$  TE elements.<sup>[50]</sup>



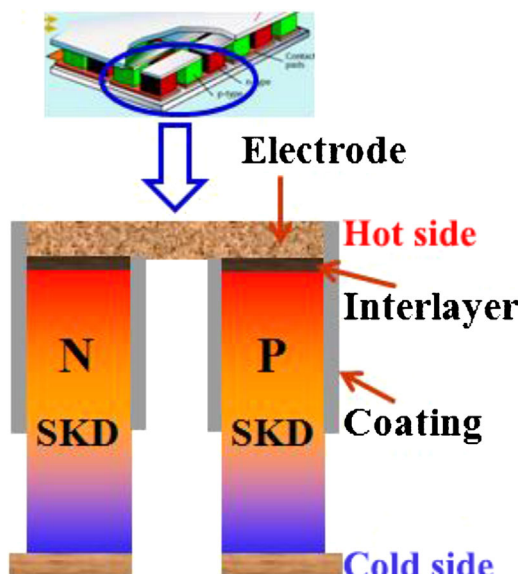


Fig. 4. Schematic diagram of a typical  $\Pi$ -shaped TE uni-couple, taking the SKD-based TE uni-couple as an example.

### 2.3.2. Thermal Spraying

Thermal spraying is a new technology to fabricate TE elements and modules.<sup>[51,52]</sup> As shown in Figure 5, TE materials are diced into the desired size and then inserted in a preformed framework which is made from a polymer or ceramics, depending on the intended operation temperature of the module. Compared with the solder method, thermal spraying has some advantages. First, the absence of gaps in the preformed framework virtually eliminates any interwall shorts between TE elements. Second, the metallization of TE elements and their integration in the module can be accomplished simultaneously. The process is simple, efficient and has good scalability. Third, modules with TE elements integrated within the preformed framework are believed to have higher strength than the traditional modules assembled with ceramic tops and bottoms to support the structure. Finally, as compared with the soldered BT modules, the BT modules fabricated by directly spraying the interface layer and the electrode (usually either Mo and Al) onto the TE materials can operate at much higher temperatures because the Al/Mo/BT joints have much high stability at high

temperatures than do solders with lower melting points. Therefore, the conversion efficiency of the sprayed modules is enhanced due to the higher temperature difference, making them suitable for power generation applications such as the recovery of vehicle exhaust heat.<sup>[53]</sup>

### 2.3.3. Diffusion Welding

Another feasible method to fabricate TE devices is the diffusion welding. With this method, a process called “one-step sintering” has been successfully developed to fabricate SKD-based TE elements and uni-couples.<sup>[54–57]</sup> The electrode material, the barrier layer material and the SKD powder are put into a graphite die, and an additional sheet is used to separate p- and n-legs for uni-couple fabrication (see Figure 6). The die assembly is then heated by employing a hot press or by using a spark plasma sintering method. The resulting sandwich structure consisting of the electrode material, the barrier layer material and the SKD powder was sintered and welded simultaneously in this process.<sup>[58]</sup>

## 2.4. Development of Testing Technology for TE Devices

The performance of a TE device is usually evaluated by its power output and conversion efficiency. Early in 1958, Harman derived a general expression for the overall efficiency of multistage cascade modules through a one-dimensional heat flow balance model.<sup>[59]</sup> He also figured out the optimal p-n pair number ratio in a two-stage module for a given intermediate junction temperature. In 1994, a large-temperature difference apparatus was designed and built for TE performance evaluation of gradually-segmented composite elements by Kisara et al.<sup>[60]</sup> The apparatus can simultaneously measure the Seebeck voltage, electrical resistance, temperature profiles and heat flux through a specimen during the same thermal cycles. In 1998, Rowe et al. developed a procedure to assess the potential of TE modules used for electrical power generation.<sup>[45]</sup> According to this method, the performance of TE modules was evaluated based on their power output, conversion efficiency and reliability, while the potential for improving their performance was investigated in terms of the power-per-area, cost-per-watt and the manufacture quality factor. Nevertheless, it is unfortunate that on today’s market there are still few available mature instruments to evaluate TE elements and modules, especially for devices intended for operation at high temperatures. A few home-built systems to evaluate the performance of high temperature modules have been developed at various laboratories. For example, Rauscher et al. developed a novel approach to measure TE modules with their set-up.<sup>[61]</sup> An alternative approach which overcomes problems regarding calibration, temperature measurement and heat loss is to determine the heat production instead of measuring the electrical power. Takazawa et al. developed a technique to accurately measure both the heat flow rate through a module

Table 1. BT-based and SKD-based TE modules made by the soldering technique.

Solder alloys	TE materials	Type	Electrode	Barrier layer	Ref.
Bi-Sn	BT	n-type	Cu	Ni	[47]
Pb-Sn	BT	n-type	Cu	Ni	[47]
Sn-37Pb	BT	p-type	Cu	Ni	[48]
Sn-4Ag-0.5Cu	BT	n-type	Cu	Ni	[48]
Pb <sub>0.3</sub> Sn <sub>0.5</sub> Ag <sub>1.5</sub>	BT	n-type	Cu	Ni	[49]
Fluxless Zn <sub>78</sub> Al <sub>22</sub>	Yb <sub>3</sub> Co <sub>4</sub> Sb <sub>12</sub>	n-type	Cu	Pd	[50]
Fluxless Zn <sub>78</sub> Al <sub>22</sub>	CexFe <sub>3</sub> CoSb <sub>12</sub>	p-type	Cu	Pd	[50]

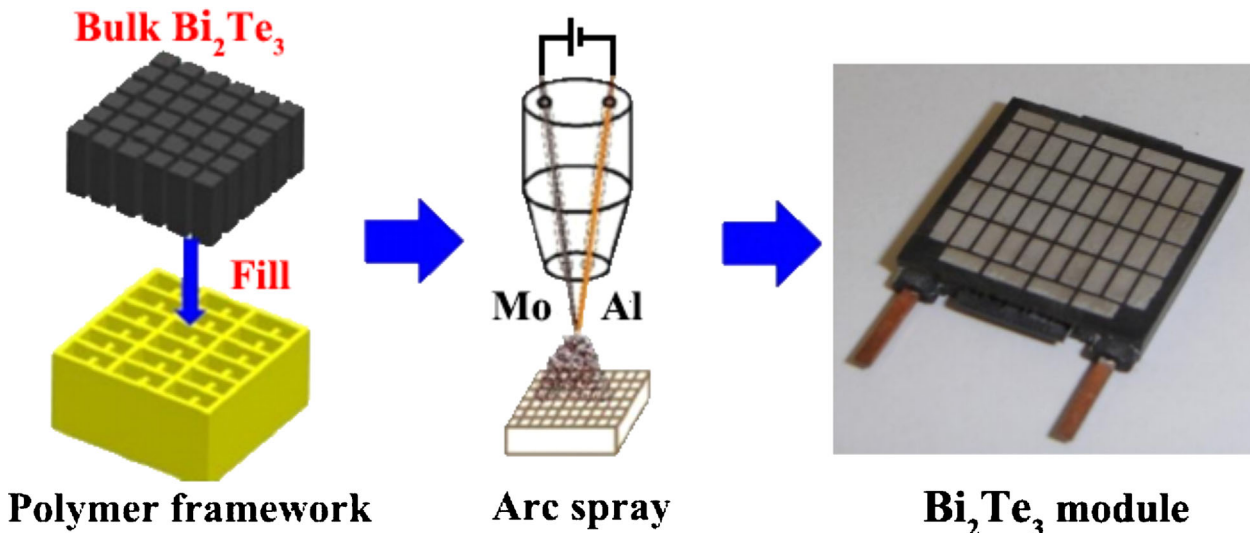


Fig. 5. Schematic diagram showing fabrication of  $\text{Bi}_2\text{Te}_3/\text{Mo}/\text{Al}$  TE device by arc spraying.

and the generated electrical power for modules operating across the temperature difference of  $277^\circ\text{C}$ .<sup>[62]</sup>

When it comes to evaluating the reliability of TE devices, the rate with which the conversion efficiency decreases may be employed. However, in practice, the effectiveness is not great due to the fact that the measurement of conversion efficiency is more difficult than that of the power output. Figure 7 shows our home-made apparatus for the isothermal and thermal cycle evaluation of TE devices. It can conveniently measure both the electrical properties and the power output of a TE uni-couple subjected to various temperature differences. There are two kinds of conditions for measuring the rate of electrical power output degradation: aging at a fixed temperature gradient across the element and aging under thermal cycling at the hot side. Based on the accelerated aging tests under harsher conditions such as higher operation temperatures, one can discern the essential

factors which have the dominant influence on the degradation of TE elements or modules. The evolution regularity of the dominant factor could help to predict the lifetime of TE devices. Unfortunately, there are few common measurement protocols and very few commercially available systems (for example, PEM made by ULVAC-RIKO In. Co.) for evaluating the rate of electrical output decrease. Typically, one encounters a number of uncertain technical issues and the evaluation protocols should be clarified and standardized according to the demands of industrial applications. For example, how many thermal cycles should the TE device withstand? How long should the cycling time be? What is the range of temperature fluctuations at the hot side? Certainly, the determination of the above as well as related parameters is closely relevant to practical applications. Moreover, modules used for different applications should

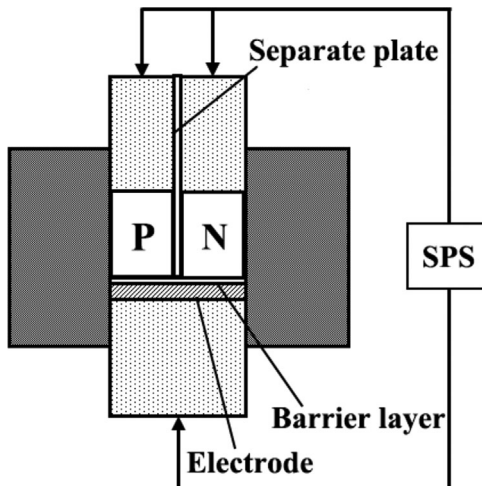


Fig. 6. Schematic diagram of the one-step sintering of SKD-based TE uni-couples.

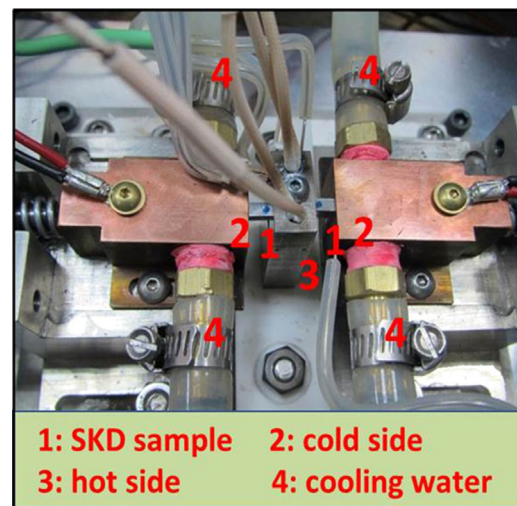


Fig. 7. A home-made apparatus for the isothermal and thermal cycle evaluation of TE devices.

be evaluated according to different standards appropriate to specific conditions of such applications.

### 3. Development of Filled-Skutterudite-Based Devices for Power Generation

In recent years many research institutions including Jet Propulsion Laboratory (JPL) in USA, GM Global Research & Development in USA, National Institute of Advanced Industrial Science and Technology in Japan, Shanghai Institute of Ceramics (SIC) in China, Fraunhofer-Institute for Physical Measurement Techniques in Germany, etc., have begun to conduct an intensive research and development of  $\text{CoSb}_3$ -based TE power generation modules due to the outstanding performance of filled and/or doped skutterudite (SKD) materials. Table 2 summarizes the available SKD-based devices reported so far. Undeniably, great progress has been made in the development of high-performance SKD-based devices for power generation. However, to be ready for large-scale applications, there are still some challenges and technical problems waiting to be solved.

#### 3.1. Electrode and Interface

##### 3.1.1. Electrode Fabrication for SKD-Based Modules

Electrode fabrication is one of the key enabling techniques in the construction of TE modules for practical applications. The importance of an electrode material is not only reflected in the TE power output, but also in the module reliability. The interface between the electrode and the TE material frequently bears a thermal shock in practical applications which usually leads to the failure of the TE module. The selection of electrodes for TE devices should follow some specific criteria: 1) excellent matching of thermal expansion coefficients (CTE) between the electrode and the TE material is the first important consideration in the construction of modules, because the CTE difference might generate cracks which affect the TE performance and the thermal stability; 2) the electrode should have high electrical and thermal conductivity so as to decrease energy dissipation; 3) at the operating temperature range, there should be no serious interdiffusion nor any chemical reactions between the electrode and TE materials, thus ensuring the TE performance is unaffected; 4) it should be easy to bond the electrode with TE materials, forming a joint with high strength and low interfacial thermal and electrical resistances; and 5) high thermal stability and low thermal stresses at the interface are important for the long-term use.

SKD-based devices are usually subjected to the operation temperature higher than 500 °C, making them vulnerable to cracks due to the mismatch in CTE and severe diffusion reaction between the metal electrode and SKD materials. Consequently, the electrode selection and the bonding process in which the electrode is joined to SKD materials in TE devices

Table 2. A summary of the reported SKD-based devices.

Materials of p-legs	Materials of n-legs	Type	Electrode of hot side	Barrier layer	Electrode of cold side	Dimension of elements	Open-circuit voltage	$P_{\max}$	$\Phi_{\max} / \text{W}$	$\Delta T / ^\circ\text{C}$	Ref.
$\text{CeFe}_{3.5}\text{Co}_{0.5}\text{Sb}_{12}$	$\text{CoSb}_3$	Uni-couple	metallic	none	metallic	20.3 mm in length	204.2 mV	1.62 W	10.65	47–627	[63]
$\text{CeFe}_{3.5}\text{Co}_{0.5}\text{Sb}_{12}$	$\text{CoSb}_3$	Uni-couple	metallic	none	metallic	20.3 mm in length	204.2 mV	0.67 W	10.7	27–700	[64]
$\text{Ce}_{0.45}\text{Co}_{2.5}\text{Fe}_{1.5}\text{Sb}_{12}$	$\text{Yb}_{0.25}\text{Co}_{4}\text{Sb}_{12}/\text{Yb}_{2}\text{O}_3$	2 pairs	Mo–Cu	Mo	Cu	Φ5 mm × 10 mm	0.21 V	0.14 W	6.4	47–537	[65]
$\text{In}_{0.25}\text{Co}_{3.0}\text{Fe}_{1.0}\text{Sb}_{12}$	$\text{In}_{0.25}\text{Co}_{3.05}\text{Ni}_{0.05}\text{Sb}_{12}$	Uni-couple	Mo–Cu	Mo–Cu	Cu	Φ10 mm × 10 mm	143 mV	0.796 W	—	55–598	[66]
$\text{La}_{0.7}\text{Ba}_{0.1}\text{Ga}_{0.1}\text{Ti}_{0.1}\text{Fe}_{3}\text{Co}_{1}\text{Sb}_{12}$	$\text{Yb}_{0.3}\text{Ca}_{0.1}\text{Al}_{0.1}\text{Ga}_{0.1}\text{In}_{0.1}\text{Co}_{3.75}\text{Fe}_{0.25}\text{Sb}_{12}$	32 pairs	Co–Fe–Ni	Co–Fe–Ni	Cu	5 mm × 5 mm × 7.6 mm	4.8 V	32 W	8	50–600	[67,68]
$\text{Ce}_{0.8}\text{Fe}_{3}\text{CoSb}_{12}$	$\text{Yb}_{0.36}\text{Co4Sb}_{12}$	9 pairs	Cu	Pd	Cu	1.7 mm × 1.7 mm × 2 mm	0.5 V	0.157 W	—	27–392	[69]
$\text{NdFe}_{3.5}\text{Co}_{0.5}\text{Sb}_{12}$	$\text{Yb}_{0.35}\text{Co4Sb}_{12}$	Uni-couple	Co–Si	—	—	—	—	—	—	70–550	[70]
$\text{Mn}_{0.8}\text{Fe}_{3}\text{CoSb}_{12}$	$\text{Ba}_{8}\text{Ga}_{16}\text{Ge}_{30}$	7 pairs	Ni	Ni	Cu	≈0.4 mm <sup>2</sup> × 6 mm	53.7 mV	124(mW cm <sup>-2</sup> )	9.1	50–300	[71]
$\text{Mn}_{0.7}\text{Fe}_{3.5}\text{Co}_{0.5}\text{Sb}_{12}$	$\text{Eu}_{8}\text{Ga}_{16}\text{Ge}_{30}$	6 pairs	Ni	Ni	Cu	≈0.6 mm <sup>2</sup> × 6 mm	53.8 mV	178(mW cm <sup>-2</sup> )	1–2	50–300	[71]
$\text{Mn}_{0.30}\text{Co}_{2.54}\text{Fe}_{1.46}\text{Sb}_{12}$	$\text{Yb}_{0.09}\text{Ba}_{0.05}\text{La}_{0.05}\text{Co}_{3.75}\text{Fe}_{0.25}\text{Sb}_{12}$	32 pairs	Al	Mo	Al	4 mm × 4 mm × 7 mm	2.73 V	10.5 W	≈7	40–500	[72,73]
$\text{La}_{0.8}\text{Ba}_{0.1}\text{Ga}_{0.1}\text{Ti}_{0.1}\text{Fe}_{3}\text{CoSb}_{12}$	$\text{La}_{0.5}\text{Ca}_{0.1}\text{Al}_{0.1}\text{Ga}_{0.1}\text{In}_{0.2}\text{Co}_{3.75}\text{Fe}_{0.25}\text{Sb}_{12}$	32 pairs	—	—	—	5 mm × 5 mm × 7.6 mm	4.92 V	32 W	8	50–600	[74]

intended to operate at high temperatures become more challenging. In 2003, researchers at JPL adopted the solid-solid contact approach to solve the joining problem of SKD/electrode in TE uni-couples whereby the contact was maintained by compression springs.<sup>[75]</sup> Consequently, the high interfacial electrical resistance and thermal resistance significantly decreased the output power and efficiency of their TE device.<sup>[76–78]</sup> Fan et al. attempted to join metallic Mo to CoSb<sub>3</sub> by spark plasma sintering.<sup>[79]</sup> The results showed that, due to the CTE mismatch between Mo and CoSb<sub>3</sub>, cracks were generated at the Mo/CoSb<sub>3</sub> interface region during a long operation at high temperatures. To achieve a good match between CoSb<sub>3</sub> and the Cu-based electrode, Zhao et al. adjusted the Cu content of Mo–Cu alloy.<sup>[80]</sup> Figure 8 presents simulation results of the residual thermal stress of three kinds of CoSb<sub>3</sub>/Ti/Mo–Cu structures by using the finite element simulation.<sup>[81]</sup> The thermal stress as shown is mainly concentrated at the interface area of CoSb<sub>3</sub>/Ti/Mo–Cu, and CoSb<sub>3</sub>/Ti/Mo<sub>50</sub>Cu<sub>50</sub> shows the smallest thermal stress among the three joints. After continuous development and improvement, Mo–Cu alloys have become generally accepted as good electrode materials because of their tunable CTE that matches SKD materials.

Beyond that, there are also other relevant research results. For example, Wojciechowski et al. developed a brazing technique for fabricating a high temperature joint ( $T_{\max} = 527^{\circ}\text{C}$ ) between the Cu electrode and CoSb<sub>3</sub>.<sup>[82]</sup> Zhao et al. attempted to minimize the CTE difference between the electrode and CoSb<sub>3</sub> by using an electrode made from the W–Cu alloy.<sup>[83]</sup>

### 3.1.2. Design of the Barrier Layer

Antimony, the major element of SKD materials, can react with most electrode materials such as Cu, Mo, Ni, and their alloys, resulting in intermetallic compounds (IMC) that decrease the efficiency and reliability of TE devices. Hence, a

barrier layer is typically required to prevent interdiffusion between the electrodes and SKD materials as well as to facilitate a “bonding” function. Fan et al. invented an interesting approach to join SKD to Mo electrodes by inserting a thin titanium interlayer using a two-step spark plasma sintering.<sup>[79,84]</sup> The results showed that an intermediate layer of TiSb formed at the Ti–CoSb<sub>3</sub> interface and a composition-gradient alloy layer was found at the Ti–Mo interface. CoSb<sub>3</sub> was effectively bonded to Mo through the insertion of the Ti barrier layer. Afterward, it was found that using a Ti foil as a substitute for the Ti powder one could further improve the joining technique.<sup>[85]</sup> Besides, Wojciechowski et al. reported the use of Mo, Ni, and Cr<sub>80</sub>Si<sub>20</sub> as the barrier layer in the Cu–CoSb<sub>3</sub> junctions.<sup>[82]</sup> Guo et al. adopted Co–Fe–Ni alloys as the diffusion barrier.<sup>[67]</sup> Song et al. investigated the performance of Au, Pt, and Ti as diffusion barrier layers, with a  $\approx 2.5\text{-}\mu\text{m-thick-layer}$  of each metal deposited by a DC sputtering method on the CoSb<sub>3</sub> leg.<sup>[86]</sup> Their results suggested that depositing a Ti thin layer onto CoSb<sub>3</sub> via sputtering could form an IMC layer at the CoSb<sub>3</sub>/Ti interface, enhancing the efficiency of CoSb<sub>3</sub>-based TE modules. Comparatively, Ti has been regarded as one of the most feasible barrier layer materials for the SKD-based TE joints in terms of the ease of bonding. However, good stability and easy bonding are usually technically contradictory. The high activity of Ti interlayer benefits the sintering and bonding between CoSb<sub>3</sub> and Mo–Cu electrodes, however, it causes degradation due to the further inter-diffusion during high-temperature operation.

Based on continuous explorations, it has been found that, in the Ti–Al binary system, there exist several electrically conductive compounds with high thermal stability, which are known to easily form through a solid-state reaction.<sup>[87]</sup> The Ti–Al alloy layer possesses the following advantages: 1) it maintains high reaction activity during sintering; 2) it suppresses activity after sintering or during high-temperature

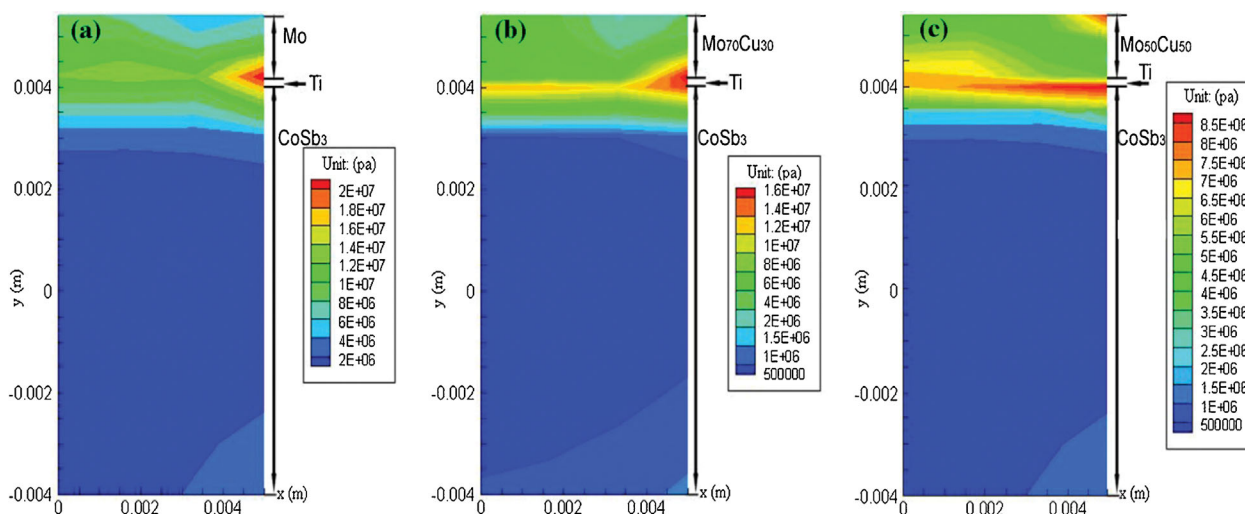


Fig. 8. Simulation results of the residual thermal stress of three kinds of CoSb<sub>3</sub>/electrode combinations by using the finite element simulation. (a) Mo electrode, (b) Mo<sub>70</sub>Cu<sub>30</sub> electrode, (c) Mo<sub>50</sub>Cu<sub>50</sub> electrode.

service due to the formation of stable  $Ti_xAl$ ; and 3) it does not raise the interfacial thermal/electrical resistance, while it maintains a good bonding strength. Experimental results indicated that  $Ti_3Al$  and  $TiAl$  alloys grew on the surface of Ti particles, forming the  $Ti/Ti_3Al/TiAl$  core/shell structure after sintering or during the operations at high temperatures. Ti/Al metals possessed high activity and enabled reaction and bonding during sintering.<sup>[87]</sup>

### 3.1.3. Interfacial Behavior and the Reliability of Joints

The interfacial reaction products, such as IMC, can exert significant effects on the mechanical properties and reliability of joints.<sup>[88–90]</sup> The interfacial structure of high-temperature joints of the  $CoSb_3$ -based TE devices is influenced by the thermochemical reaction, which closely relates to the reliability of TE devices.<sup>[57]</sup> Therefore, to have a clear picture of the interfacial behavior and to evaluate the reliability of TE joints at high temperatures, aging studies are necessary. Zhao et al. studied the interfacial microstructure and reliability of the  $CoSb_3/Ti/Mo-Cu$  joints during a thermal duration test.<sup>[57]</sup> As shown in Figure 9, a three-layer structure of  $TiSb/TiSb_2/TiCoSb$  resulting from the mutual diffusion of Sb and Ti is observed at the  $CoSb_3/Ti$  interface after thermal aging at 550 °C for 30 days. By using a four-point probe device, the  $CoSb_3/Ti/Mo-Cu$  interface electrical resistivity of about 20  $\mu\Omega\text{cm}^2$  was measured prior to thermal aging, and it increased to 28  $\mu\Omega\text{cm}^2$  after aging at 550 °C for 20 days.<sup>[91]</sup> In addition, a multi-layer heat transfer model combined with the laser perturbation method

(Netzsch, LFA427, multi-layer model) has been adopted to calculate and evaluate the interface thermal resistance of the  $CoSb_3/Ti/Mo-Cu$  structure.<sup>[91]</sup> The contact thermal conductivity reaches  $1.6 \times 10^4 \text{ Wm}^{-2} \text{ K}^{-1}$  before thermal aging and  $1.4 \times 10^4 \text{ Wm}^{-2} \text{ K}^{-1}$  after thermal aging at 550 °C for 20 days. The effective interfacial thermal conductance shows a declining trend with increasing temperature and falls from 17.5 to 15  $\text{Wm}^{-1} \text{ K}^{-1}$  after aging at 550 °C for 30 days.<sup>[91]</sup>

The growth of interlayers can be used as one of the criteria for judging the service life of TE devices. Figure 10a shows the total thickness of IMC layers of the  $CoSb_3/Ti/Mo-Cu$  joint under different aging temperatures and time. It is found that the total thickness of IMC layers linearly increases with the square root of aging time. The maximum life of the  $CoSb_3/Ti/Mo-Cu$ -based TE device is predicted to be less than 23 years assuming that  $T_H$  is kept at  $\approx 500^\circ\text{C}$ .<sup>[57]</sup> Figure 10b shows the shear strength of the  $CoSb_3/Ti/Mo-Cu$  joint as a function of aging temperature and time. The shear strength significantly decreases after accelerated aging during the initial 120 h and then slightly decreases with further prolonged aging. Ultimately, even after aging at 575 °C for 720 h, the shear strength still has a value of about 12.6 MPa.<sup>[57]</sup>

Depressing the growth of IMC layers is considered important to improve the service reliability and to prolong the service life. Figure 11 shows the SEM images of the  $Ti_{100-x}Al_x/Yb$ -SKD interfacial microstructure after aging at 600 °C for 16 days in vacuum.<sup>[87]</sup> Compared with the  $Ti/Yb$ -SKD system, interfacial diffusion in the  $Ti-Al/Yb$ -SKD system is obviously restrained and any degradation of the bonding strength is effectively suppressed at an appropriate Al content

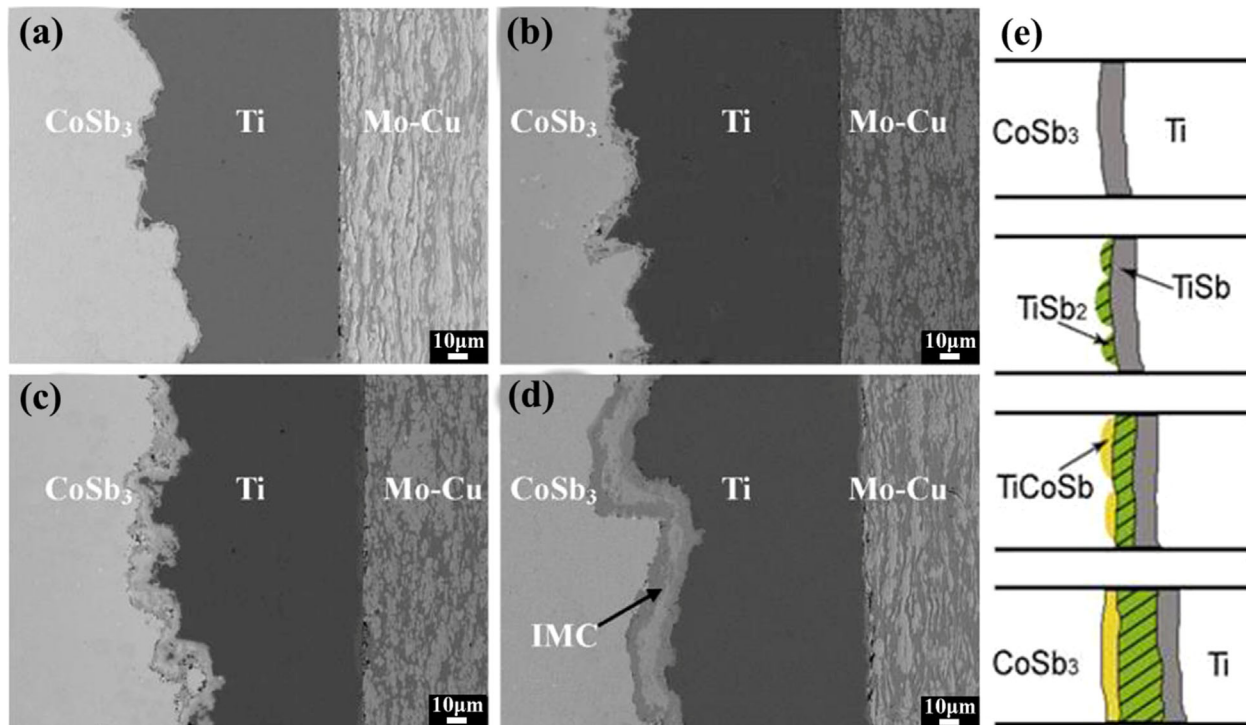


Fig. 9. SEM images of  $CoSb_3/Ti/Mo-Cu$  interface aged at 550 °C for different aging time: (a) 0 day, (b) 8 days, (c) 20 days and (d) 30 days. (e) Schematic diagram of the  $CoSb_3/TiSb_2/TiSb/Ti$  structure formed at the  $CoSb_3/Ti$  interface.<sup>[57]</sup> Copyright 2009, Elsevier.

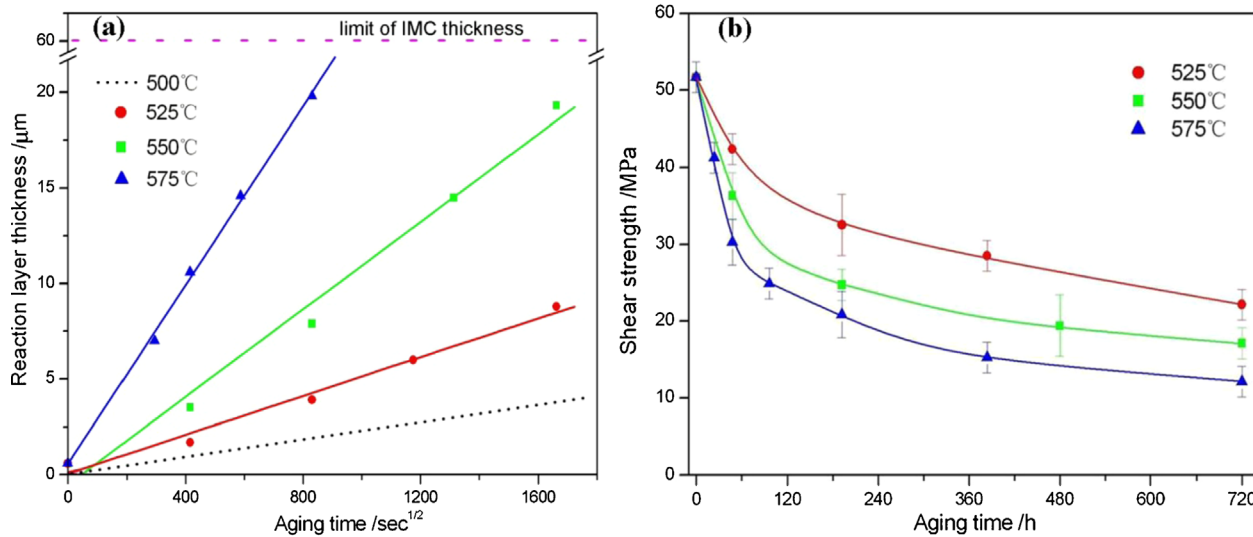


Fig. 10. (a) Total thickness of intermetallic compounds of the  $\text{CoSb}_3/\text{Ti}/\text{Mo}-\text{Cu}$  joint as a function of aging temperature and time, (b) shear strength of the  $\text{CoSb}_3/\text{Ti}/\text{Mo}-\text{Cu}$  joint as a function of aging temperature and time.<sup>[57]</sup> Copyright 2009, Elsevier.

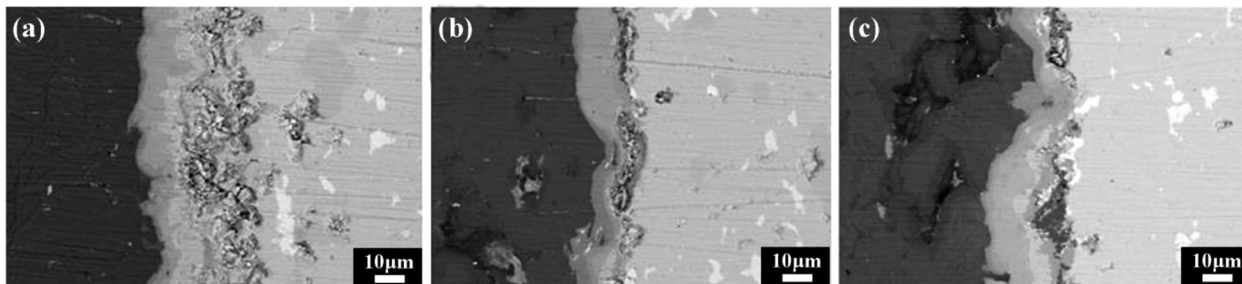


Fig. 11. SEM images of the  $\text{Ti}_{100-x}\text{Al}_x/\text{Yb}$ -SKD interfacial microstructure after aging at  $600^\circ\text{C}$  for 16 days in vacuum: (a)  $x = 0$ , (b)  $x = 6$ , (c)  $x = 12$ .<sup>[87]</sup> Copyright 2014, Elsevier.

of  $\approx 6$  at%.<sup>[87]</sup> With a further increase of the Al content, however, the interfacial diffusion is promoted. After aging at  $600^\circ\text{C}$  for 16 days in vacuum, there was no (or very minor) formation of a brittle  $\text{TiCoSb}$  phase at the interface, indicating that the formation of  $\text{TiCoSb}$  intermetallic layer is effectively prevented by Ti-Al alloying.<sup>[87]</sup>

Figure 12a summarizes the evolution of the diffusion layer thickness in  $\text{Ti}_{100-x}\text{Al}_x/\text{Yb}$ -SKD joints as a function of the aging time.<sup>[87]</sup> It is clear that the growing speed of the diffusion layer has been greatly decreased after alloying Ti and Al. The interfacial diffusion and reactions are sensitive to the Al content in the Ti-Al barrier layer. Figure 12b shows the evolution of the contact resistivity as a function of the aging time for the Ti-Al/Yb-SKD joints. As for the Ti interlayer, the contact resistivity ( $\rho_c$ ) after aging increases by a factor of 12 of its initial value, however,  $\rho_c$  changes much less in the Ti-Al alloying interlayer system than in the pure Ti interlayer system. Therefore, suitable Al content in the Ti-Al barrier layer not only effectively depresses the interfacial diffusion

between the Ti-Al barrier layer and Yb-SKD, but also greatly improves the stability of the contact resistivity.

### 3.2. Protection Coating for Preventing Sb Sublimation and Oxidation

A series of studies have revealed that  $\text{CoSb}_3$ -based SKD materials undergo oxidation and Sb sublimation at temperatures  $>400^\circ\text{C}$ .<sup>[92–100]</sup> This is especially a problem with p-type

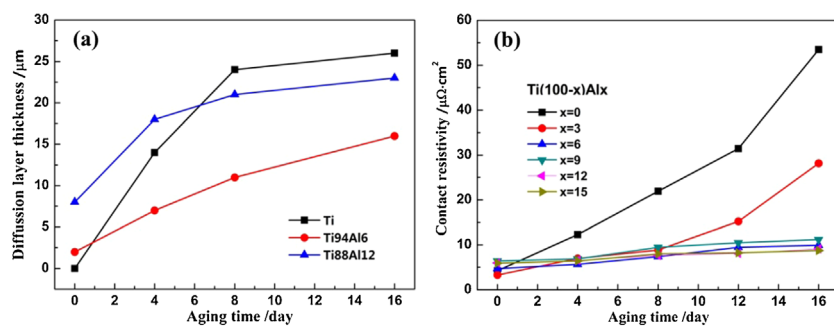


Fig. 12. (a) Diffusion layer thickness as a function of the aging time for different Ti-Al/Yb-SKD joints aged at  $600^\circ\text{C}$ , (b) the contact resistivity as a function of the aging time for the Ti-Al/Yb-SKD joints aged at  $600^\circ\text{C}$ .

$\text{CoSb}_3$ -based SKD ( $\text{M}_y\text{Fe}_x\text{Co}_{4-x}\text{Sb}_{12}$ ). The troublesome oxidation would completely incapacitate the element in a short service period. When operating at the service temperature,  $\text{CoSb}_3$ -based SKD and filled SKD materials are also vulnerable to decomposition by sublimation of Sb atoms which would change the composition of TE materials and eventually resulting in the degradation of the TE performance. Moreover, the sublimation products can diffuse or condense on the cold-side of TE uni-couples, leading to electrical shorts in the TE device.<sup>[98]</sup> The poor oxidation resistance of SKD materials and Sb sublimation at elevated temperatures seriously limit their large-scale applications.<sup>[101,102]</sup>

Creating a protective coating on TE materials is considered an effective and reliable way of preventing SKD materials to oxidize and Sb to sublime. Coating materials including metallic films, ceramic coatings, enamel, aerogels, and multi-layer/composite coatings have been reported. For example, El-Genk et al. reported that metallic (Mo, V, Ta, Ti) coatings could effectively suppress the sublimation of Sb in  $\text{CoSb}_3$ -based SKDs.<sup>[63,64,103]</sup> Sakamoto et al. adopted a continuous metal foil as a physical barrier which restrained thermal decomposition near the surface of SKD materials.<sup>[104]</sup> Godlewski et al. deposited Cr-5Si thin layers onto  $\text{CoSb}_3$  using pulse magnetron sputtering, preventing the degradation of SKDs at high temperatures in air.<sup>[105]</sup> However, the thin layers lost their protection ability at 600 °C. Generally speaking, most metallic coatings applied by sputtering adhere poorly to SKDs. If this were not so, significant inter-diffusion and reactions between the coating and the substrate would likely be unavoidable.<sup>[102]</sup> As for ceramics and enamel layers, the mismatch in the CTE between the coating layer and SKDs is difficult to eliminate. Sakamoto et al. then developed a thick aerogel coating to suppress Sb sublimation in vacuum.<sup>[106]</sup> Although, the aerogel coatings have an ultra-low thermal conductivity and good adhesion to SKDs, the low strength and brittleness of aerogels present new challenges regarding their mechanical reliability. Furthermore, the interconnected micropores or mesopores in the aerogels may provide a migration pathway to Sb vapor and oxygen, which may cause gradual degradation during the long-term operation.

Afterward, Dong et al. fabricated inorganic-organic silica-based composite protective coatings dispersed with glass or alumina granular particles for SKD TE materials via a modified sol-gel procedure combined with a slurry-blade method.<sup>[107,108]</sup> Their results showed that the formation of micro-cracks was restrained by either glass particles or alumina particles during solidification due to the relaxation of tremendous cohesive stresses in the gel. After thermal aging at 600 °C in vacuum, inter-diffusion of Sn from the glass to SKDs and of Sb from SKDs to the coating layer was observed in the silica-based composite coatings with dispersed glass particles. On the other hand, neither diffusion nor reactions between the coating and SKD materials were found upon using alumina particles dispersed in silica-based composite coatings. Recently, Dong et al. adopted a new glass-based composite coating in which silica-based aerogel

particles were used as an enforcement phase and organic silane was added as a cross-linking binder to realize the protective effect on the surface of SKDs.<sup>[99]</sup> High-temperature oxidation tests showed that the glass-coated SKDs possessed good resistance to both oxidation and Sb sublimation.

To simultaneously solve the Sb sublimation problem and SKDs oxidation at high temperatures, our team put forward a multi-layer structure coating consisting of a dense inner metallic film and an outer thicker oxide layer.<sup>[109,110]</sup> Xia et al. attempted to deposit a Mo/SiO<sub>x</sub> multilayer film on the p-type Ce<sub>0.9</sub>Fe<sub>3</sub>CoSb<sub>12</sub> SKD surface as a protective coating by magnetron sputtering.<sup>[110]</sup> A thermal aging test was conducted under vacuum at 550–650 °C. The microstructural evolution of the multilayer film showed that the inter-diffusion of Mo and Sb at the boundary at high temperatures resulted in the formation of a Mo<sub>3</sub>Sb<sub>7</sub> layer that was stable at high temperatures. This not only facilitated the adhesion improvement between SKD and Mo/SiO<sub>x</sub>, but also blocked further inter-diffusion at the boundary. The sublimation of Sb in Ce<sub>0.9</sub>Fe<sub>3</sub>CoSb<sub>12</sub> at high temperatures was greatly suppressed by the Mo/SiO<sub>x</sub>/Mo<sub>3</sub>Sb<sub>7</sub> multilayer coating. Based on these results, we fabricated a more efficient three-layer coating: Mo/SiO<sub>x</sub>/glass-ceramic. As shown in Figure 13, the mass gain due to oxidation in air at 600 °C is greatly depressed by the Mo/SiO<sub>x</sub>/glass-ceramic three-layer coating. However, the fabrication of overlaid coatings for SKDs remains a considerable challenge.

### 3.3. Evaluation of the Output Performance and Service Behavior

The basic performance measurement of a TE power generation module includes the power output and the conversion efficiency as a function of temperature and applied temperature difference. Guo et al. reported the performance of a SKD-based module with the size of 50 × 50 × 7.6 mm<sup>3</sup>.<sup>[67,74]</sup> The modules exhibited generation performance of 32 W of power output and 8% conversion efficiency. After heating/cooling cycles between 600 and 200 °C with further continuous

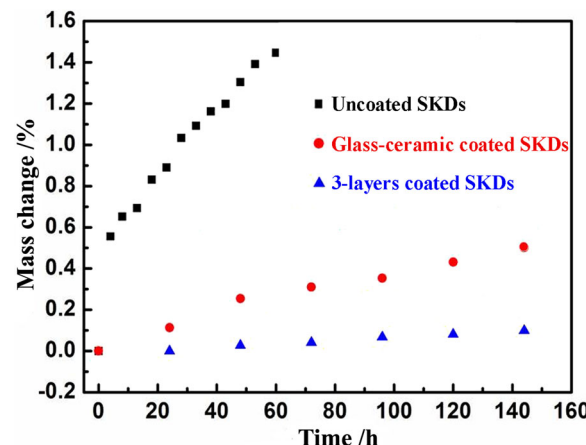


Fig. 13. The mass change of SKDs upon aging at 600 °C in air with or without coating as a function of time.

heating at 600 °C for 240 h in vacuum, no change of the module's power generation performance was observed. Jorge et al. reported a SKD-based device fabricated using commercially available solder alloys and metal barriers.<sup>[50]</sup> The module showed an output volume power density higher than 1.5 W cm<sup>-3</sup> under the temperature difference of 365 °C and an internal resistance and specific contact resistivity of 0.7 Ω and 4.77 × 10<sup>-4</sup> Ω cm<sup>2</sup>, respectively. The conversion efficiency was, however, not reported. During thermocycling, the internal module resistance was significantly affected due to the damage in the contacts. Recently, we fabricated SKD-based modules with different size using p-type Ce<sub>y</sub>Fe<sub>x</sub>Co<sub>4-x</sub>Sb<sub>12</sub> and n-type Yb<sub>0.3</sub>Co<sub>4</sub>Sb<sub>12</sub>. As shown in Figure 14a, the maximum power output reached 10.12 W and the corresponding conversion efficiency attained 6.65% at the temperature difference of 556 °C when the element size was 4.5 × 6 × 8 mm<sup>3</sup> and the size of the SKD-based module with 10 pairs was 30 × 30 × 10 mm<sup>3</sup>. For another module design of 50 × 50 × 10 mm<sup>3</sup> consisting of 32 pairs of 5 × 5 × 7.5 mm<sup>3</sup> elements, the maximum power output reached 25.08 W and the corresponding conversion efficiency increased to 7.3% at the temperature difference of 510 °C (see Figure 14b). Salvador et al. then reported on measurements of both the power output and the thermal-to-electrical energy conversion efficiency carried out on an upgraded TE module system built at the Fraunhofer Institute for Physical Measurement Techniques.<sup>[73]</sup> The results demonstrated that a 32 couple SKD-based module could supply 11.5 W of electricity under a temperature difference of 460 °C, which corresponded to an extrapolated value of 7.5% conversion efficiency.

The performance of TE modules can be enhanced by stacking together multiple TE modules creating the so-called cascade modules. Such modules can incorporate TE materials with the optimal figure of merit achieved at different temperatures, thus broadening the operational range of the device.<sup>[111]</sup> El-Genk et al. produced efficient Bi<sub>2</sub>Te<sub>3</sub>/CoSb<sub>3</sub> segmented TE uni-couples, reaching the conversion efficiency of 12% at 550 °C and having the contact resistivity of about

50 μΩ cm<sup>2</sup>. At 670 °C the device achieved 15% conversion efficiency, more than doubling that of a SiGe-based single stage TE devise of comparable size.<sup>[112]</sup> Kajikawa et al. reported 10% conversion efficiency achieved with their Bi<sub>2</sub>Te<sub>3</sub>/CoSb<sub>3</sub> cascaded module under the temperature difference of 400 °C.<sup>[113]</sup> Recently, we fabricated BT-SKD cascade modules, as is shown in Figure 15. The maximum conversion efficiency of 10.1% has been obtained with the temperature difference of 500 °C.

For the long-term service behavior, the isothermal and thermal cycle evaluations were conducted on the CoSb<sub>3</sub>-based devices by using our home-made apparatus (see Figure 7). The power output for an isothermally aged uni-couple consisting of p-type Ce<sub>y</sub>FeCo<sub>3</sub>Sb<sub>12</sub> and n-type Yb<sub>0.3</sub>Co<sub>4</sub>Sb<sub>12</sub> under 25 °C for T<sub>C</sub> and 500 °C for T<sub>H</sub> shows that it is steady for 35 days or more (see Figure 16a). After thermal cycling over 2400 times under 25 °C for T<sub>C</sub> and 100–550 °C oscillating for T<sub>H</sub>, the power output of the n-type element remained steady and the power output of the P-N couple showed a small drop at the beginning of the test, but afterward maintained its steady value (see Figure 16b). In addition, long-term evaluation of the II-shaped CoSb<sub>3</sub>-based uni-couple was performed under an argon atmosphere with a partial pressure of 280 Pa. The results shown in Figure 17 indicate that all measured parameters, including the open circuit voltage, power output, load resistance, and T<sub>H</sub>, remained generally stable after more than 8 000 h.

## 4. Development of BT-Based Devices For Power Generation

### 4.1. Optimization of the Joints of BT-Based Devices

In commercial TE modules, the solder is usually employed to bond BT columns to the electrodes. Cu, Al, and Ag can be used as electrode materials at the hot side in BT modules.<sup>[114,115]</sup> Some solders, such as Sn-Bi, Sn-Pb, and Sn-Ag

alloys, are commonly employed in assembling TE modules.<sup>[116,117]</sup> However, Sn-based solders have a low melting point and modules using this solder should not be exposed to temperatures exceeding about 200 °C. Moreover, operating as a power generator under temperatures close to 200 °C for long periods of time may result in serious diffusion problems and reactions between the solder and the TE material at the hot end of the module, affecting the service life and stability of the device.<sup>[118–121]</sup> Lan et al. attempted to plate a nickel diffusion barrier layer onto the BT-based surface in order to prevent mutual diffusion and chemical reactions between the solder and BT, and then soldered a copper electrode onto the

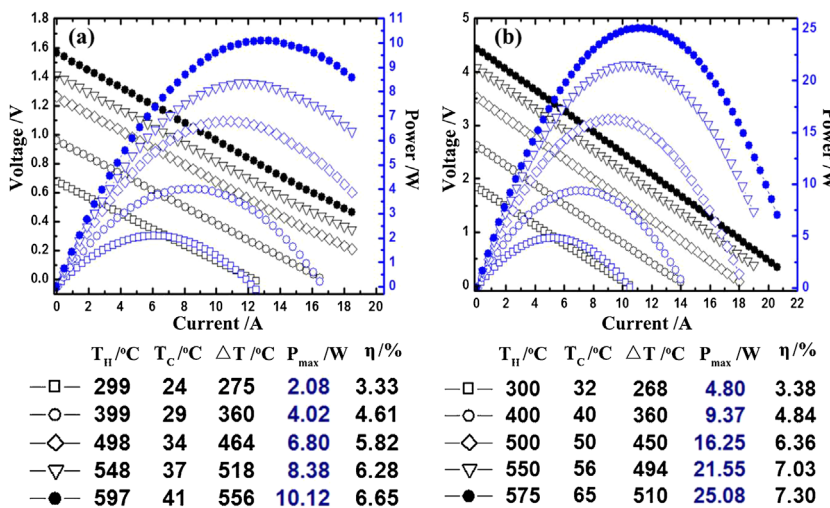


Fig. 14. (a) P-I-V curves of the SKD-based module consisting of 10 pairs of couples at different temperatures, (b) P-I-V curves of the SKD-based module consisting of 32 pairs of couples at different temperature.

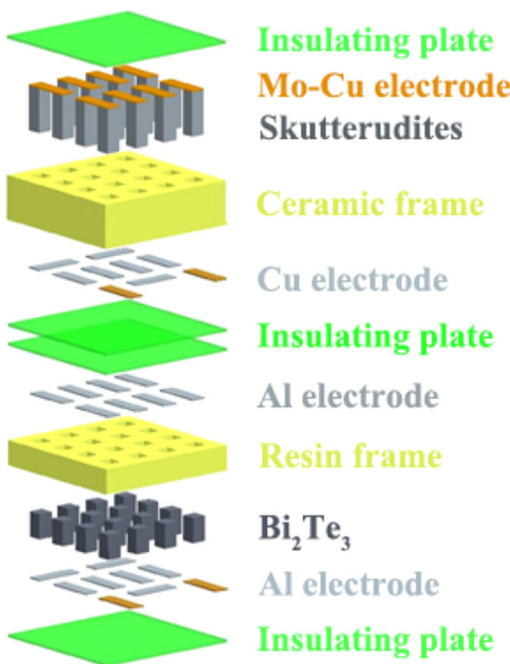


Fig. 15. Schematic diagram depicting fabrication of a BT-SKD cascade module.

nickel layer.<sup>[122]</sup> However, diffusion of nickel into BT occurred during the soldering process which resulted in a mechanically weak bonding and consequent degradation of the device's performance. Basically identical results concerning the failure of deposited Ni to prevent inter-diffusion between Cu and BT following annealing at 200 °C were also obtained by Lyore et al.<sup>[123]</sup> Chen's team reported on the preparation of a metalized nickel layer on both n- and p-type BT-based nanostructured legs by sputtering for the solar thermoelectric generators.<sup>[124,125]</sup> However, sputtering is not an easy process for the production of thick nickel layers.<sup>[126]</sup> An electrochemical deposition process was, therefore, adopted to prepare a thicker nickel layer.<sup>[120,127]</sup> However, weak interface bonding

between Ni and the TE material may lead to a severe device degradation. Liu et al. then directly pressed a Ni powder layer onto a BT-based powder layer by hot pressing.<sup>[126]</sup> A significantly improved bonding strength was achieved in both n-type Ni/Bi<sub>2</sub>Te<sub>2.7</sub>Se<sub>0.3</sub> and p-type Ni/Bi<sub>0.4</sub>Sb<sub>1.6</sub>Te<sub>3</sub> legs. Nevertheless, a large contact resistivity of  $\approx 210 \mu\Omega \text{ cm}^2$  was observed in the n-type legs while the contact resistivity of p-type legs was less than  $1 \mu\Omega \text{ cm}^2$ . On the other hand, Lin et al. investigated Pd, Ni/Au, Ag, and Ti/Au as diffusion barrier layers, finding that Ti/Au formed the best diffusion barrier for BT elements among the four candidates.<sup>[114]</sup> After annealing at 250 °C for 200 h, the thickness of the Ti/Au layers was merely 200 nm and the Ti/Au layers exhibited an excellent step coverage on the rough BT surface. However, such inter-layers have the high cost and require a complex preparation process. Recently, Li et al. chose metallic Sb, one of the elements in Bi<sub>2</sub>Te<sub>3</sub>, as the interlayer, and fabricated Bi<sub>2</sub>Te<sub>3</sub>/Sb and Bi<sub>2</sub>Se<sub>3</sub>/Sb TE joints by SPS.<sup>[128]</sup> The prepared Sb-TE joint showed better electrical contact and reliability compared with the solder formed TE joint. The contact resistivity of the Bi<sub>2</sub>Te<sub>3</sub>/Sb/Bi<sub>2</sub>Te<sub>3</sub> joint was  $3 \mu\Omega \text{ cm}^2$  before aging and increased modestly with the increasing aging time in vacuum, reaching  $8.5 \mu\Omega \text{ cm}^2$  after aging for 30 days at 300 °C. The increase was associated with the increased thickness of the Sb<sub>2</sub>Te<sub>3</sub> diffusion layer formed at the Bi<sub>2</sub>Te<sub>3</sub>/Sb interface.

#### 4.2. Fabrication and Evaluation of BT-Based Devices Made by Arc-Spraying

As mentioned, the application of soldered BT devices for power generation is restricted as far as the operation temperature and the service life is concerned. Arc spraying is a cost-effective technology during which any heat deformation is far less troublesome than in plasma spraying, thus reducing the rate of defective products. Using this method, Li et al. was able to make joints between aluminum electrodes and BT materials with a molybdenum barrier

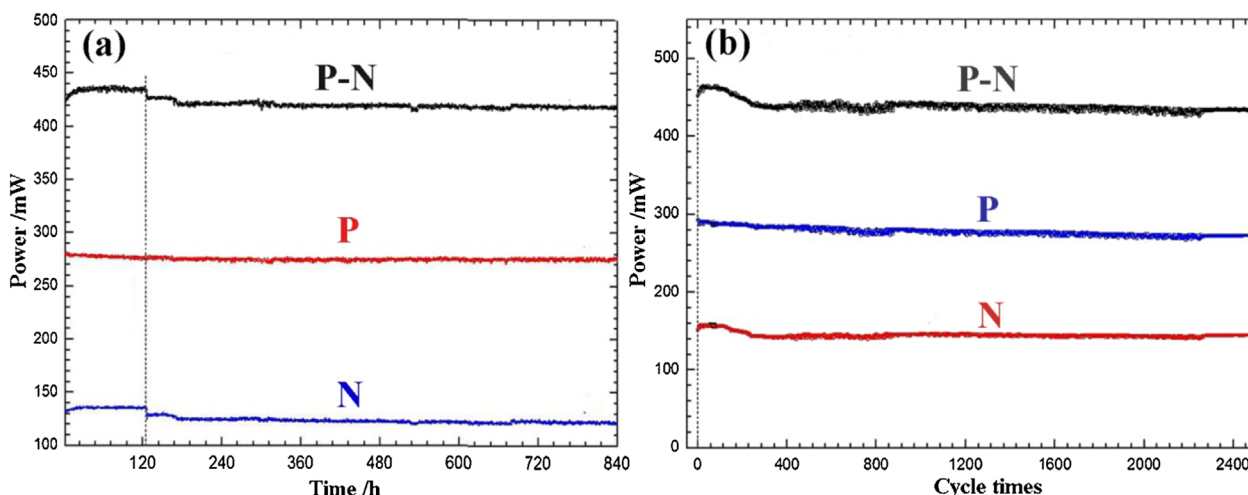


Fig. 16. Evaluation of a TE uni-couple consisting of p-type Ce<sub>y</sub>FeCo<sub>3</sub>Sb<sub>12</sub> and n-type Yb<sub>0.3</sub>Co<sub>4</sub>Sb<sub>12</sub>. (a) Power output for isothermal aging as a function of time under 25 °C for  $T_C$  and 500 °C for  $T_H$ , (b) power output for thermal cycling as a function of cycle times under 25 °C for  $T_C$  and 100–550 °C oscillating for  $T_H$ .

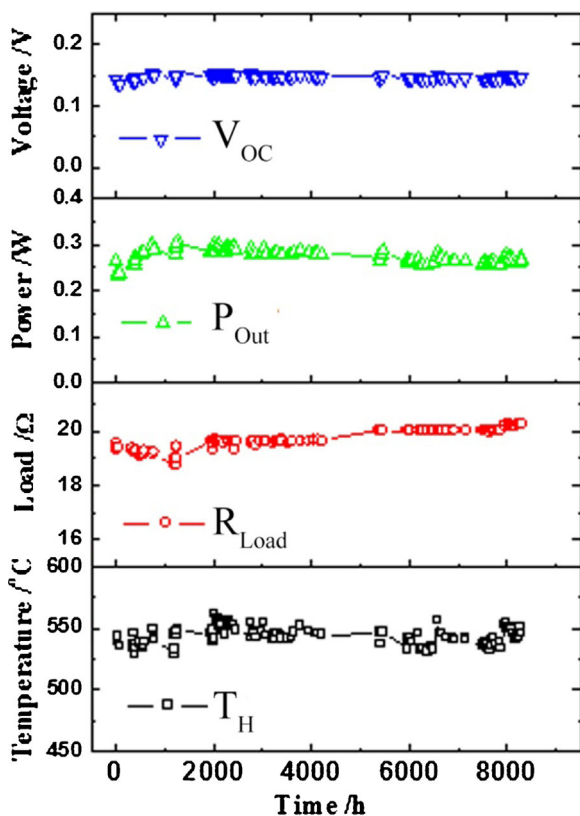


Fig. 17. Results of the long-term evaluation of a  $\Pi$ -shaped  $\text{CoSb}_3$ -based uni-couple as a function of time.

layer.<sup>[129,130]</sup> They reported a relatively large interfacial resistivity of about  $80 \mu\Omega \text{ cm}^2$  for their BT/Mo/Al joints, comparable to the interfacial resistivity of BT joints made using the soldering method.<sup>[53]</sup> The aging test was conducted to characterize the stability of the BT/Mo/Al joints at high temperatures. Figure 18a–c shows SEM images of the BT/Mo/Al joint after the vacuum isothermal aging test at  $300^\circ\text{C}$  for 4, 10, and 20 days, respectively.<sup>[53]</sup> The microstructural evolution indicates that each interface maintained its good bonding after aging for 10 days, and no inter-diffusion or chemical reactions were observed. However, after aging for 20 days, a small number of cracks appeared at the interface, even though good interface bonding was still kept. Thermal shock tests were conducted by aging at  $300^\circ\text{C}$  for 10 min followed by cooling in ice water for 5 min in one cycle. The results in Figure 18d–f show that the BT/Mo/Al joint had good interface adhesion and favorable stability, but cracks were observed in SEM images after the thermal shocks repeated for 10 and 30 cycles. Big differences in the CTE of Al, Mo, and BT resulted in the formation of cracks at the interfaces after thermal shocks, certainly a negative influence from the perspective of long-term use.

Compared with the Al electrode, copper has a higher electrical conductivity and thermal conductivity, and the CTE of copper is closer to that of BT-based materials. By replacing Al electrodes with copper, a BT/Mo/Cu joint has also been fabricated by arc-spraying.<sup>[131]</sup> The Mo barrier layer of  $1\mu\text{m}$  to  $1\text{mm}$  in thickness was arc-sprayed on the BT blocks and then a Cu electrode was arc-sprayed with the thickness of  $0.1-$

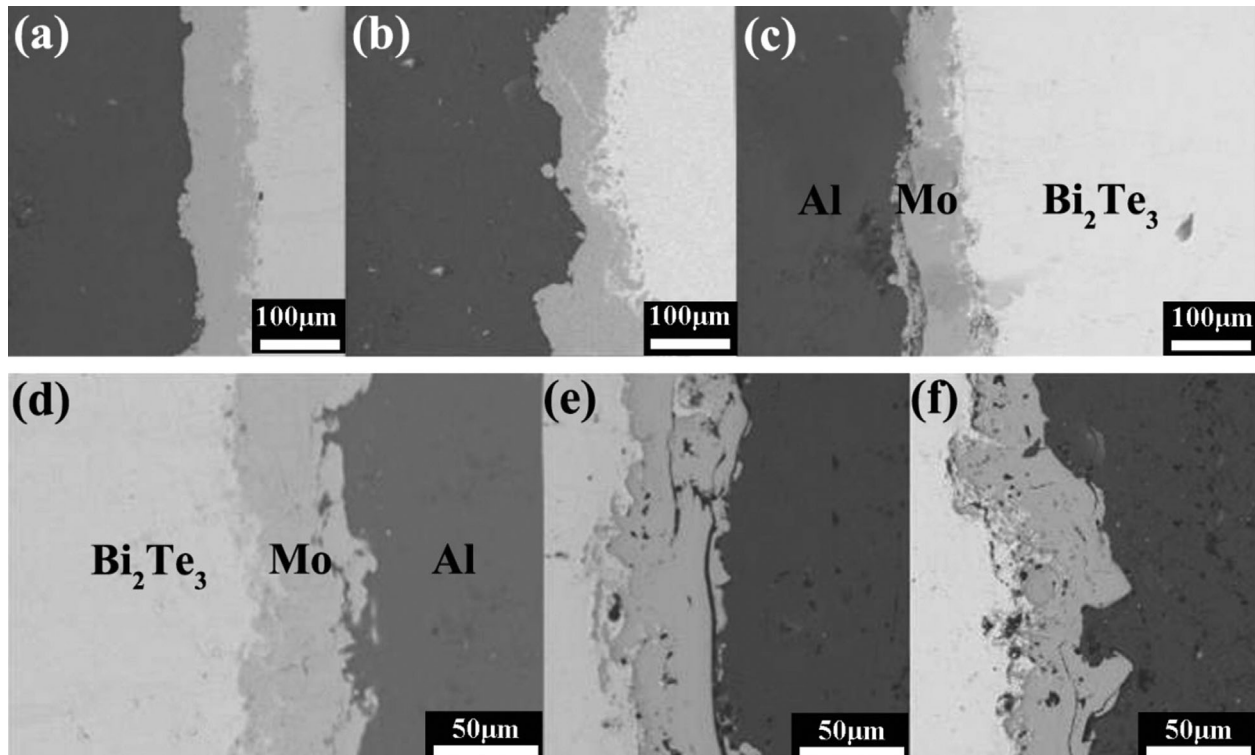


Fig. 18. SEM images of the  $\text{Bi}_2\text{Te}_3/\text{Mo}/\text{Al}$  element aged for (a) 4 days, (b) 10 days and (c) 20 days at  $300^\circ\text{C}$ ; SEM images of the  $\text{Bi}_2\text{Te}_3/\text{Mo}/\text{Al}$  TE element thermally shocked (aged at  $300^\circ\text{C}$  for 10 min followed by cooling in ice water for 5 min) for (d) 0, (e) 10 and (f) 30 cycles.

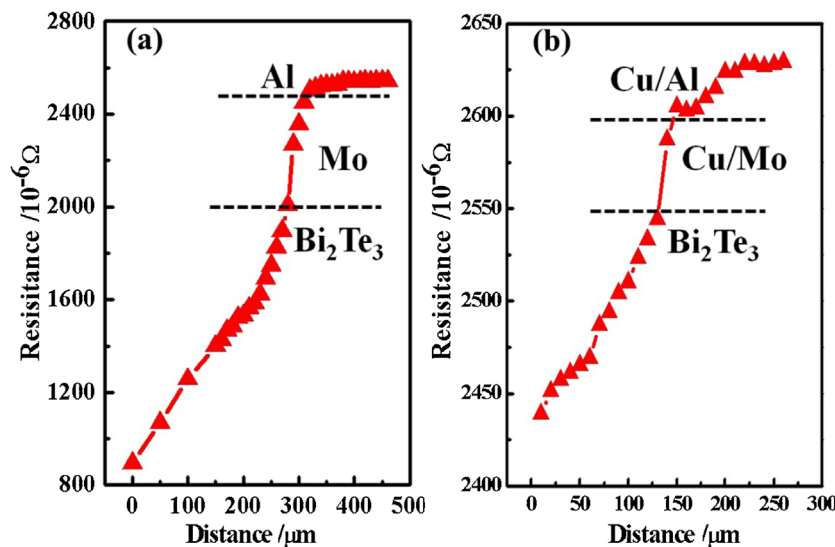


Fig. 19. Contact resistance of (a) Bi<sub>2</sub>Te<sub>3</sub>/Mo/Al and (b) Bi<sub>2</sub>Te<sub>3</sub>/Mo/Cu/Al elements.

10 mm. The joint had better conductivity and good interface stability. However, because Cu is prone to oxidation at high temperatures, it should not be used directly as an electrode in power generation modules but is more suitable as a stress buffer layer. Al has a greater oxidation resistance because a layer of dense alumina forms on the surface of Al which blocks any further oxygen intake. A modified joint structure consisting of BT/Mo/Cu/Al was then fabricated by arc-spraying.<sup>[53]</sup> Figure 19 compares the contact resistance of the modified BT/Mo/Cu/Al joint structure with that of the BT/Mo/Al joint. The interfacial resistance of BT/Mo/Cu/Al was about 50  $\mu\Omega$ , dropping by almost 90% compared with that of BT/Mo/Al.

Two kinds of BT/Mo/Al and BT/Mo/Cu/Al TE modules with the same size ( $58 \times 60 \times 6 \text{ mm}^3$ ) consisting of 49 pairs of couples (n-type Bi<sub>2</sub>Se<sub>0.3</sub>Te<sub>2.7</sub> and p-type Bi<sub>0.5</sub>Sb<sub>1.5</sub>Te<sub>3</sub>) with the size of elements of  $4.15 \times 4.15 \times 4.5 \text{ mm}^3$  were evaluated by P-I measurements.<sup>[53]</sup> As shown in Figure 20, the maximum

power output was 2.9 W at the current of 2.75 A for the BT/Mo/Al TE device, while the maximum power output reached 4.6 W at the current of 3.25 A for the BT/Mo/Cu/Al TE device, an improvement of over 50% after the interlayer was modified.

For the evaluation of reliability, an accelerated thermal aging test was conducted on the BT/Mo/Al and BT/Mo/Cu/Al modules, respectively.<sup>[53,132]</sup> By conducting accelerated aging tests on the BT/Mo/Al TE device, its service life was estimated as about 8 years at the hot side temperature of 260 °C, assuming that the device failure will occur when the resistance change rate rises to 10%.<sup>[53,132]</sup> To test the durability of the BT module, 15 heating/cooling cycles with heating to 100–150–200 °C and then cooling down to 200–150–100 °C were applied on the BT/Mo/Al TE

device. Figure 21 shows the power output performance of the BT/Mo/Al TE device during these heat/cooling cycles. No change in the module's power output was observed. These results indicate that arc-sprayed BT-based devices have excellent thermal stability and are suitable for power generation applications.<sup>[53]</sup>

Furthermore, Bai et al. have recently invented a BT-based TE device for the TE power generation system intended for the use in cars and trucks, which has a copper damping layer between the BT base layer and the molybdenum barrier layer and has a copper stress buffer layer formed between the molybdenum barrier layer and the aluminum electrode layer.<sup>[132]</sup> The copper damping layer is plated on BT blocks by the arc spraying or plasma spraying process. The molybdenum barrier layer, the copper stress buffer layer and the aluminum electrode layer are successively plated by arc spraying. This BT-based TE device features a low contact resistance and high stability.<sup>[132]</sup>

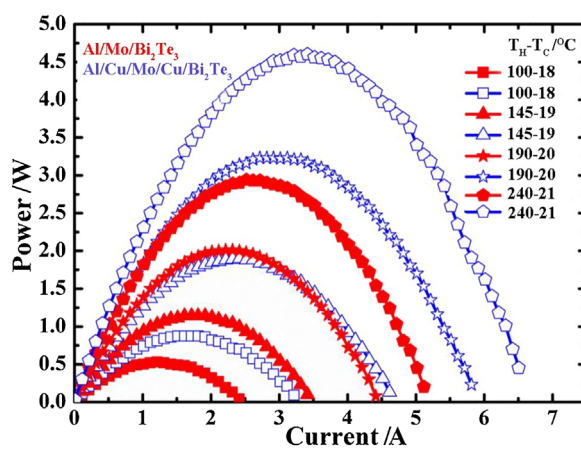


Fig. 20. P-I curves of the BT/Mo/Al and BT/Mo/Cu/Al TE module at different temperatures.

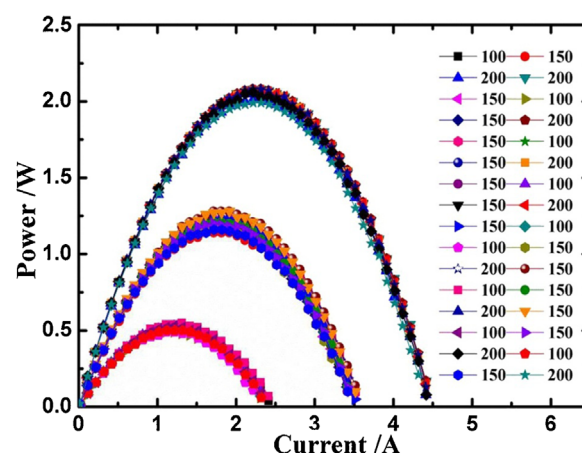


Fig. 21. P-I curves of the BT/Mo/Al TE module during thermal cycle testing.

## 5. Conclusion and Outlook

Thermoelectric conversion has long been recognized as a potentially transformative power generation technology and is now growing rapidly due to the ability to develop cost-effective, pollution-free, solid-state-based conversion of heat into electricity. Recent achievements with the bismuth telluride-based and skutterudites-based TE devices have expedited the steps to practical applications of TE-based power generation. In this paper, we presented an overview on the advances and pointed out the bottlenecks for a large scale TE power generation in terms of the efficiency of operation and the service behavior. The design principle, fabrication methods and testing technology of TE devices were summarized. Particular attention was paid to the skutterudites-based and bismuth telluride-based TE devices intended for power generation applications.

The module fabrication techniques for TE power generation are becoming mature and reliable and developing towards the mass production. The evaluation results indicate that the power generation performance of TE devices is gradually being improved. However, when it comes to meeting the needs for industrial applications, challenges still lie ahead and much more needs to be done in the future. First of all, the conversion efficiency is in need of further improvements and the module fabrication cost awaits further reductions through scaling up and process optimization. Second, a strategy to improve the reliability of the device operating at high temperatures and high oxygen environment is required for practical applications. The service behavior under real and complex operation conditions (vibration, oxidation, thermal circling, etc.) should be further investigated in detail. Furthermore, the lack of accurate measurement protocols and the scarcity of mature and reliable instrumentation for evaluation of the TE elements and modules have created another barrier. A systematic method for the prediction of life cycle and reliability of operation should be established by combining the service behavior including electrical, mechanical and thermal performances of materials and devices. All in all, continued efforts from various fields are required to gain a more thorough understanding of the rational design, cost-effective fabrication, and evaluation of optimized TE materials and modules which should accelerate the use of TE technology in wide ranges of power generation applications.

Article first published online: September 22, 2015

Manuscript Revised: July 29, 2015

Manuscript Received: June 30, 2015

- [1] D. M. Rowe, in *CRC Handbook of Thermoelectrics* (Ed: D. M. Rowe), CRC Press, Boca Raton, FL, USA **1995**, Ch. 1.
- [2] M. S. El-Genk, H. H. Saber, in *CRC Handbook of Thermoelectrics: Micro to Nano* (Ed: D. M. Rowe), CRC Press, Boca Raton, FL, USA **2006**, Ch. 43.

- [3] J. H. Yang, T. Caillat, *MRS Bull.* **2006**, *31*, 224.
- [4] A. Bulusua, D. G. Walker, *Superlattices Microst.* **2008**, *44*, 1.
- [5] H. J. Goldsmid, R. W. Douglas, *Br. J. Appl. Phys.* **1954**, *5*, 386.
- [6] A. Ioffe, *Semiconductors Thermoelements and Thermoelectric Cooling*, Infosearch Ltd., London **1957**.
- [7] A. J. Minnich, M. S. Dresselhaus, Z. F. Ren, G. Chen, *Energy Environ. Sci.* **2009**, *2*, 466.
- [8] M. S. Dresselhaus, G. Chen, M. Y. Tang, R. G. Yang, H. Lee, D. Z. Wang, Z. F. Ren, J. P. Fleurial, P. Gogna, *Adv. Mater.* **2007**, *19*, 1043.
- [9] L. D. Hicks, M. S. Dresselhaus, *Phys. Rev. B* **1993**, *47*, 2727.
- [10] L. D. Hicks, T. C. Harman, M. S. Dresselhaus, *Appl. Phys. Lett.* **1993**, *63*, 3230.
- [11] D. T. Morelli, T. Caillat, J. P. Fleurial, A. Borshchevsky, J. Vandersande, B. Chen, C. Uher, *Phys. Rev. B: Condens. Matter Mater. Phys.* **1995**, *51*, 9622.
- [12] T. Caillat, A. Borshchevsky, J. P. Fleurial, *J. Appl. Phys.* **1996**, *80*, 4442.
- [13] L. D. Hicks, T. C. Harman, X. Sun, M. S. Dresselhaus, *Phys. Rev. B Condens. Matter Mater. Phys.* **1996**, *53*, R10493.
- [14] G. Chen, *Phys. Rev. B Condens. Matter Mater. Phys.* **1998**, *57*, 14958.
- [15] T. Koga, X. Sun, S. B. Cronin, M. S. Dresselhaus, *Appl. Phys. Lett.* **1998**, *73*, 2950.
- [16] G. S. Nolas, D. T. Morelli, T. M. Tritt, *Annu. Rev. Mater. Sci.* **1999**, *29*, 89.
- [17] T. M. Tritt, *Science* **1999**, *283*, 804.
- [18] B. Poudel, Q. Hao, Y. Ma, Y. C. Lan, A. Minnich, B. Yu, X. Yan, D. Z. Wang, A. Muto, D. Vashaee, X. Y. Chen, J. M. Liu, M. S. Dresselhaus, G. Chen, Z. F. Ren, *Science* **2008**, *320*, 634.
- [19] X. Shi, J. Yang, J. R. Salvador, M. F. Chi, J. Y. Cho, H. Wang, S. Q. Bai, J. H. Yang, W. Q. Zhang, L. D. Chen, *J. Am. Chem. Soc.* **2011**, *133*, 7837.
- [20] H. L. Liu, X. Shi, F. F. Xu, L. L. Zhang, W. Q. Zhang, L. D. Chen, Q. Li, C. Uher, T. Day, G. J. Snyder, *Nat. Mater.* **2012**, *11*, 422.
- [21] Y. He, T. Day, T. S. Zhang, H. L. Liu, X. Shi, L. D. Chen, G. J. Snyder, *Adv. Mater.* **2014**, *26*, 3974.
- [22] N. Shutoh, S. Sakurada, *J. Alloys Compd.* **2005**, *38*, 204.
- [23] S. Sakurada, N. Shutoh, *Appl. Phys. Lett.* **2005**, *86*, 082105.
- [24] H. Muta, T. Kanemitsu, K. Kuroasaki, S. Yamanaka, *Mater. Trans.* **2006**, *47*, 1453.
- [25] K. Biswas, J. Q. He, I. D. Blum, C. Wu, T. P. Hogan, D. N. Seidman, V. P. Dravid, M. G. Kanatzidis, *Nature* **2012**, *489*, 414.
- [26] L. D. Zhao, S. H. Lo, Y. S. Zhang, H. Sun, G. J. Tan, C. Uher, C. Wolverton, V. P. Dravid, M. G. Kanatzidis, *Nature* **2014**, *508*, 373.
- [27] H. Alam, S. Ramakrishna, *Nano Energy* **2013**, *2*, 190.

- [28] L. L. Cai, *Master Dissertation of Wu Han University of Technology, China* **2011**.
- [29] G. W. Wang, X. F. Wang, C. L. Yu, H. T. Jiang, J. H. Li, S. T. Chen, *Mater. Rev.* **2007**, *21*, 115.
- [30] J. F. Fan, L. D. Chen, S. Q. Bai, X. Shi, *Mater. Lett.* **2004**, *58*, 3876.
- [31] Z. W. Ruan, L. S. Liu, P. C. Zhai, P. F. Wen, Q. J. Zhang, *J. Electron. Mater.* **2010**, *39*, 2029.
- [32] M. H. Elsheikh, D. A. Shnawah, M. F. M. Sabri, S. B. M. Said, M. H. Hassan, M. B. A. Bashir, M. Mohamad, *Renew. Sust. Energ. Rev.* **2014**, *30*, 337.
- [33] S. Chen, Z. F. Ren, *Mater. Today* **2013**, *16*, 387.
- [34] S. LeBlanc, S. K. Yee, M. L. Scullin, C. Dames, K. E. Goodson, *Renew. Sust. Energ. Rev.* **2014**, *32*, 313.
- [35] F. J. DiSalvo, *Science* **1999**, *285*, 30.
- [36] L. E. Bell, *Science* **2008**, *321*, 1457.
- [37] S. Kumar, S. D. Heister, X. F. Xu, J. R. Salvador, G. P. Meisner, *J. Electron. Mater.* **2013**, *42*, 665.
- [38] M. Zebarjadi, K. Esfarjani, M. S. Dresselhaus, Z. F. Ren, G. Chen, *Energ. Environ. Sci.* **2012**, *5*, 5147.
- [39] S. B. Riffat, X. L. Ma, *Appl. Therm. Eng.* **2003**, *23*, 913.
- [40] A. Schmitz, C. Stiewe, E. Muller, *J. Electron. Mater.* **2013**, *42*, 1702.
- [41] G. Min, in *CRC Handbook of Thermoelectrics: Micro to Nano* (Ed: D. M. Rowe), CRC Press, Boca Raton, FL, USA **2006**, Ch. 11.
- [42] D. T. Crane, L. E. Bell, *Proceedings of 25th International Conference on Thermoelectrics*, Vienna, Austria **2006**.
- [43] G. J. Snyder, in *CRC Handbook of Thermoelectrics: Micro to Nano* (Ed: D. M. Rowe), CRC Press, Boca Raton, FL, USA **2006**, Ch. 9.
- [44] D. M. Rowe, G. Min, *IEE P Sci. Meas. Tech.* **1996**, *143*, 351.
- [45] D. M. Rowe, G. Min, *J. Power Sources* **1998**, *73*, 193.
- [46] C. C. Li, Z. X. Zhu, L. L. Liao, M. J. Dai, C. K. Liu, C. R. Kao, *Sci. Technol. Weld. Joi.* **2013**, *18*, 421.
- [47] R. J. Buist, S. J. Roman, *Proceedings of the 18th International Conference on Thermoelectrics*, Baltimore, USA **1999**.
- [48] C. N. Liao, C. H. Lee, W. J. Chen, *Electrochem. Solid St.* **2007**, *10*, 23.
- [49] G. C. Jorge, M. Gao, *Proceedings of the 9th European Conference Thermoelectrics*, AIP Conference Proceedings, Thessaloniki, Greece **2012**, *1449*, 454.
- [50] G. A. Jorge, V. P. Anthony, K. Andreas, V. Paz, M. Gao, *J. Electron. Mater.* **2013**, *42*, 1369.
- [51] F. A. Leavitt, J. C. Bass, N. B. Elsner, *United States Patent*, **1999**, 5856210.
- [52] Y. Q. Wu, D. P. Lu, L. F. Jiang, L. G. Chen, L. H. F., X. Y. Li, S. Q. Bai, L. D. Chen, X. Y. Huang, *Chinese Patent*, **2012**, CN101783386B.
- [53] F. Li, *Doctor Dissertation of University of Chinese Academy of Sciences, China*, **2013**.
- [54] D. G. Zhao, X. Y. Li, W. Jiang, L. D. Chen, *J. Inorg. Mater.* **2009**, *24*, 545.
- [55] D. G. Zhao, H. R. Geng, L. D. Chen, *Int. J. Appl. Ceram. Technol.* **2012**, *9*, 733.
- [56] D. G. Zhao, L. Wang, Y. H. Cai, W. Jiang, L. D. Chen, *Mater. Sci. Forum* **2009**, *610–613*, 389.
- [57] D. G. Zhao, X. Y. Li, L. He, W. Jiang, L. D. Chen, *J. Alloys Compd.* **2009**, *477*, 425.
- [58] P. F. Qiu, X. Y. Huang, L. D. Chen, M. Gu, X. Shi, X. G. Xia, Y. S. Tang, C. Wang, *Chinese Patent*, **2014**, CN103746070A.
- [59] T. C. Harman, *J. Appl. Phys.* **1958**, *29*, 1373.
- [60] K. Kisara, L. Chen, T. Sudo, N. Sakuranaka, M. Niino, in *Proceedings of the 3rd International Symposium on Structural and Functional Gradient Materials* (Ed: B. Ilischner, N. Cherradi), Polytechniques et universitaires romandes press, Lausanne **1994**, 657.
- [61] L. Rauscher, H. Kaibe, H. Ishimabushi, S. Sano, E. W. Miiller, D. Platzeck, *Proceedings of 22nd International Conference on Thermoelectrics*, Hérault, France **2003**.
- [62] H. Takazawa, H. Obara, Y. Okada, K. Kobayashi, T. Onishi, T. Kajikawa, *Proceedings of 25th International Conference on Thermoelectrics*, Vienna, Austria **2006**.
- [63] M. S. El-Genk, H. H. Saber, T. Caillat, J. Sakamoto, *Energ. Convers. Manage.* **2006**, *47*, 174.
- [64] H. H. Saber, M. S. El-Genk, T. Caillat, *Energ. Convers. Manage.* **2007**, *48*, 555.
- [65] D. G. Zhao, C. W. Tian, S. S. Tang, Y. T. Liu, L. K. Jiang, L. D. Chen, *Mat. Sci. Semicon. Proc.* **2010**, *13*, 221.
- [66] S. M. Choi, K. H. Kim, S. M. Jeong, H. S. Choi, Y. S. Lim, W. S. Seo, I. H. Kim, *J. Electron. Mater.* **2012**, *41*, 1004.
- [67] J. Q. Guo, H. Y. Geng, T. Ochi, S. Suzuki, M. Kikuchi, Y. Yamaguchi, S. Ito, *J. Electron. Mater.* **2012**, *41*, 1036.
- [68] T. Ochi, G. Nie, S. Suzuki, M. Kikuchi, S. Ito, J. Q. GUO, *J. Electron. Mater.* **2014**, *43*, 2344.
- [69] G. C. Jorge, V. P. Anthony, K. Andreas, V. Paz, M. Gao, *J. Electron. Mater.* **2013**, *42*, 1369.
- [70] A. Muto, J. Yang, B. Poudel, Z. F. Ren, G. Chen, *Adv. Energy Mater.* **2013**, *3*, 245.
- [71] E. Alleno, N. Lamquembe, R. Cardoso-Gil, M. Ikeda, F. Widder, O. Rouleau, C. Godart, Yu. Grin, S. Paschen, *Phys. Status Solidi A* **2014**, *211*, 1293.
- [72] J. R. Salvador, J. Y. Cho, Z. X. Ye, J. E. Moczygemba, A. J. Thompson, J. W. Sharp, J. D. Konig, R. Maloney, T. Thompson, J. Sakamoto, H. Wang, A. A. Wereszczak, G. P. Eisner, *J. Electron. Mater.* **2013**, *42*, 1389.
- [73] J. R. Salvador, J. Y. Cho, Z. X. Ye, J. E. Moczygemba, A. J. Thompson, J. W. Sharp, J. D. Konig, R. Maloney, T. Thompson, J. Sakamoto, H. Wang, A. A. Wereszczak, *Phys. Chem. Chem. Phys.* **2014**, *16*, 12510.
- [74] H. Y. Geng, T. Ochi, S. Suzuki, M. Kikuchi, S. Ito, J. Q. Guo, *J. Electron. Mater.* **2013**, *42*, 1999.

- [75] M. S. El-Genk, H. H. Saber, T. Caillat, *Energ. Convers. Manage.* **2003**, *4*, 1755.
- [76] H. S. Chun, J. W. S. Yoon, B. Jung, *J. Alloys Compd.* **2007**, *439*, 91.
- [77] M. S. El-Genk, H. H. Saber, T. Caillat, J. Sakamoto, *Energ. Convers. Manage.* **2006**, *47*, 174.
- [78] H. H. Saber, M. S. El-Genk, T. Caillat, *Energ. Convers. Manage.* **2007**, *48*, 555.
- [79] J. F. Fan, L. D. Chen, S. Q. Bai, X. Shi, *Mater. Lett.* **2004**, *58*, 3876.
- [80] D. G. Zhao, X. Y. Li, W. Jiang, L. D. Chen, *J. Inorg. Mater.* **2008**, *23*, 1296.
- [81] D. G. Zhao, *Doctor Dissertation of University of Chinese Academy of Sciences, China* **2009**.
- [82] K. T. Wojciechowski, R. Zybalia, R. Mania, *Micro-electron. Reliab.* **2011**, *51*, 1198.
- [83] D. G. Zhao, H. R. Geng, X. Y. Teng, *J. Alloys Compd.* **2012**, *517*, 198.
- [84] X. Li, L. D. Chen, J. Fan, S. Q. Bai, *Proceedings of 24th International Conference on Thermoelectrics*, Clemson, SC, USA **2005**.
- [85] D. G. Zhao, X. Y. Li, L. He, W. Jiang, L. D. Chen, *Intermetallics* **2009**, *17*, 136.
- [86] B. Song, S. Lee, S. Cho, M. J. Song, S. M. Choi, W. S. Seo, Y. Yoon, W. Lee, *J. Alloys Compd.* **2014**, *617*, 160.
- [87] M. Gu, X. G. Xia, X. Y. Li, X. Y. Huang, L. D. Chen, *J. Alloys Compd.* **2014**, *610*, 665.
- [88] D. Q. Yu, L. Wang, *J. Alloys Compd.* **2008**, *458*, 542.
- [89] A. Kumar, Z. Chen, *Mater. Sci. Eng. A* **2006**, *423*, 175.
- [90] P. Sun, C. Andersson, X. Wei, Z. Cheng, D. S. Guan, J. Liu, *J. Alloys Compd.* **2007**, *437*, 169.
- [91] D. G. Zhao, H. R. Geng, L. D. Chen, *Int. J. Appl. Ceram. Technol.* **2012**, *9*, 733.
- [92] P. Wei, W. Y. Zhao, C. L. Dong, X. Yang, Y. Jian, Q. J. Zhang, *Acta Mater.* **2011**, *59*, 3244.
- [93] X. G. Xia, P. F. Qiu, X. Shi, X. Y. Li, X. Y. Huang, L. D. Chen, *J. Electron. Mater.* **2012**, *41*, 2225.
- [94] J. Leszczynski, K. T. Wojciechowski, A. L. Malecki, *J. Therm. Anal. Calorim.* **2011**, *105*, 211.
- [95] E. Godlewska, K. Zawadzka, A. Adamczyk, M. Mitoraj, K. Mars, *Oxid. Met.* **2010**, *74*, 113.
- [96] D. G. Zhao, C. W. Tian, Y. T. Liu, C. W. Zhan, L. D. Chen, *J. Alloys Compd.* **2011**, *509*, 3166.
- [97] D. G. Zhao, C. W. Tian, S. Q. Tang, Y. T. Liu, L. D. Chen, *J. Alloys Compd.* **2010**, *504*, 552.
- [98] R. Hara, S. Inoue, H. T. Kaike, S. Sano, *J. Alloys Compd.* **2003**, *349*, 297.
- [99] H. L. Dong, X. Y. Li, X. Y. Huang, Y. F. Zhou, W. Jiang, L. D. Chen, *Ceram. Int.* **2013**, *39*, 4551.
- [100] P. F. Qiu, X. G. Xia, X. Y. Huang, M. Gu, Y. T. Qiu, L. D. Chen, *J. Alloys Compd.* **2014**, *612*, 365.
- [101] H. L. Dong, X. Y. Li, X. Y. Huang, Y. F. Zhou, W. Jiang, L. D. Chen, *Ceram. Int.* **2013**, *39*, 4551.
- [102] H. L. Dong, X. Y. Li, Y. S. Tang, J. Zou, X. Y. Huang, Y. F. Zhou, W. Jiang, G. J. Zhang, L. D. Chen, *J. Alloys Compd.* **2012**, *527*, 247.
- [103] H. H. Saber, M. S. El-Genk, *Energy Convers. Manage.* **2007**, *48*, 1383.
- [104] J. S. Sakamoto, T. Caillat, J. P. Fleurial, G. J. Snyder, *United States Patent*, **2009**, US7480984B1.
- [105] E. Godlewska, K. Zawadzka, K. Mars, R. Mania, K. Wojciechowski, A. Opoka, *Oxid. Met.* **2010**, *74*, 205.
- [106] J. S. Sakamoto, G. J. Snyder, T. Calliat, J. P. Fleurial, S. M. Jones, J. A. Palk, *United States Patent*, **2008**, US7461512B2.
- [107] H. L. Dong, X. Y. Li, Y. S. Tang, J. Zou, X. Y. Huang, Y. F. Zhou, W. Jiang, G. J. Zhang, L. D. Chen, *J. Alloys Compd.* **2012**, *527*, 247.
- [108] L. D. Chen, H. L. Dong, X. Y. Li, X. Y. Huang, W. Jiang, Y. S. Tang, X. G. Xia, J. C. Liao, L. He, *Chinese Patent*, **2013**, CN103146301A.
- [109] L. He, L. D. Chen, X. Y. Huang, X. Y. Li, X. G. Xia, *United States Patent*, **2012**, US20120164416A1.
- [110] X. G. Xia, X. Y. Huang, X. Y. Li, M. Gu, P. F. Qiu, J. C. Liao, Y. S. Tang, S. Q. Bai, L. D. Chen, *J. Alloys Compd.* **2014**, *604*, 94.
- [111] T. Fujisaka, H. T. Sui, R. O. Suzuki, *J. Electron. Mater.* **2013**, *42*, 1688.
- [112] M. S. El-Genk, H. H. Saber, *Energ. Convers. Manage.* **2003**, *44*, 1069.
- [113] T. Kajkawa, *Proceedings of the 20th International Conference on Thermoelectrics*, Beijing, China **2001**.
- [114] W. P. Lin, D. E. Wesolowski, C. C. Lee, *J. Mater. Sci. Mater. El* **2011**, *22*, 1313.
- [115] H. N. Y. Hiroyoshi, Y. Keiichi, U. Takusane, *Matsushita Electric Works Ltd. Japan*, **1996**.
- [116] T. D. Alieva, B. S. Barkhalov, D. S. Abdinov, *Inorg. Mater.* **1995**, *31*, 178.
- [117] C. N. Liao, C. H. Lee, W. J. Chen, *Electrochem. Solid St.* **2007**, *10*, 23.
- [118] I. V. Gasenikova, T. E. Svechnikova, *Inorg. Mater.* **2004**, *40*, 570.
- [119] S. W. Chen, C. N. Chiu, *Scripta Mater.* **2007**, *56*, 97.
- [120] T. Y. Lin, C. N. Liao, A. T. Wu, *J. Electron. Mater.* **2011**, *41*, 153.
- [121] S. W. Chen, C. Y. Wu, H. J. Wu, W. T. Chiu, *J. Alloys Compd.* **2014**, *611*, 313.
- [122] Y. C. Lan, D. Z. Wang, G. Chen, Z. F. Ren, *Appl. Phys. Lett.* **2008**, *92*, 101910.
- [123] O. D. Lyore, T. H. Lee, R. P. Gupta, J. B. White, H. N. Alshareef, M. J. Kim, B. E. Gnade, *Surf. Interface Anal.* **2008**, *41*, 440.
- [124] D. Kraemer, B. Poudel, H. P. Feng, J. C. Caylor, B. Yu, X. Yan, Y. Ma, X. W. Wang, D. Z. Wang, A. Muto, K. McEnaney, M. Chiesa, Z. F. Ren, G. Chen, *Nat. Mater.* **2011**, *10*, 532.
- [125] K. McEnaney, D. Kraemer, Z. F. Ren, G. Chen, *J. Appl. Phys.* **2011**, *110*, 074502.
- [126] W. S. Liu, H. Z. Wang, L. J. Wang, X. W. Wang, G. Joshi, G. Chen, Z. F. Ren, *J. Mater. Chem. A* **2013**, *1*, 13093.

- [127] S. P. Sheng, J. Yang, B. Poudel, B. Yu, Y. H. Chang, Z. F. Ren, G. Chen, *Phys. Chem. Chem. Phys.* **2013**, *15*, 6757.
- [128] F. Li, X. Y. Huang, W. Jiang, L. D. Chen, *J. Electron. Mater.* **2013**, *42*, 1219.
- [129] X. Y. Li, L. D. Chen, X. G. Xia, Y. S. Tang, S. Y. Tao, X. G. Xia, Y. Q. Wu, R. P. Lu, *Chinese Patent*, **2009**, CN101409324A.
- [130] X. Y. Li, L. D. Chen, X. G. Xia, Y. S. Tang, S. Y. Tao, X. G. Xia, Y. Q. Wu, R. P. Lu, *Chinese Patent*, **2010**, CN201408783Y.
- [131] S. Q. Bai, F. Lei, T. Wu, Y. Q. Wu, X. Y. Li, X. Y. Huang, L. D. Chen, *Chinese Patent*, **2014**, CN103579482A.
- [132] S. Q. Bai, F. Lei, T. Wu, X. Y. Huang, L. D. Chen, *Chinese Patent*, **2013**, CN103413889A.